© 2021. Published by The Company of Biologists Ltd | Development (2021) 148, dev196378. doi:10.1242/dev.196378

RESEARCH ARTICLE

An L-type lectin receptor-like kinase promotes starch accumulation during rice pollen maturation

Zhiyuan He[1,*], Ting Zou[1,*], Qiao Xiao[1,*], Guoqiang Yuan[1], Miaomiao Liu[1], Yang Tao[1], Dan Zhou[1], Xu Zhang[1], Qiming Deng[2], Shiquan Wang[2], Aiping Zheng[1], Jun Zhu[2], Yueyang Liang[2], Xiumei Yu[2], Aijun Wang[1], Huainian Liu[2], Lingxia Wang[2], Ping Li[2,‡] and Shuangcheng Li[1,‡]

ABSTRACT

Starch accumulation is key for the maturity of rice pollen grains; however, the regulatory mechanism underlying this process remains unknown. Here, we have isolated a male-sterile rice mutant, *abnormal pollen 1* (*ap1*), which produces nonviable pollen grains with defective starch accumulation. Functional analysis revealed that *AP1* encodes an active L-type lectin receptor-like kinase (L-LecRLK). AP1 is localized to the plasma membrane and its transcript is highly accumulated in pollen during the starch synthesis phase. RNA-seq and phosphoproteomic analysis revealed that the expression/phosphorylation levels of numerous genes/proteins involved in starch and sucrose metabolism pathway were significantly altered in the mutant pollen, including a known rice UDP-glucose pyrophosphorylase (OsUGP2). We further found that AP1 physically interacts with OsUGP2 to elevate its enzymatic activity, likely through targeted phosphorylation. These findings revealed a novel role of L-LecRLK in controlling pollen maturity via modulating sucrose and starch metabolism.

KEY WORDS: Rice, AP1, L-LecRLK, Pollen starch, Phosphorylation, OsUGP2

INTRODUCTION

The development of male gametophytes is one of the key steps in the plant reproductive process (McCormick, 2004). The development of pollen, the male gametophyte of flowering plants, starts from the differentiation of sporogenous cells and involves a series of complex events: pollen mother cells (PMCs), which are generated from sporogenous cells, undergo meiotic division (Ma, 2005). Subsequently, the individual haploid microspore with surrounding primexine is freed from the tetrads and then vacuolates into a round shape (Borg et al., 2009). Soon thereafter, with the gradual disappearance of the vacuole and the complete formation of pollen wall (consisting of the outer exine and inner intine), the microspores go through two-step mitotic division. During this stage, the accumulation of pollen starch initiates. After the second mitotic division, microspores develop into mature pollen grains (Zhang et al., 2011).

Pollen development requires a sufficient source of energy and carbohydrates (McCormick, 1991). Starch is one of the most conventional energy substances and carbohydrate source in the development of pollen; and starch is also the main storage material in the cytoplasm of mature pollen (Baker and Baker, 1979). During the last stages of pollen development, a rapid phase of starch accumulation occurring inside the microspore is crucial for pollen maturation and viability (Datta et al., 2001). This final phase not only provides the reserve of energy for pollen germination but also establishes pollen maturity, especially in many monocots (Datta et al., 2003).

The sequential starch biosynthetic pathway is well documented in the development of heterotrophic seeds (Okita, 1992; Tetlow et al., 2004). For example, sucrose is unloaded from the phloem termini into basal endosperm cells by plasma membrane-localized sucrose transporters and by SUGARS WILL EVENTUALLY BE EXPORTED TRANSPORTERs, or hydrolyzed first by cell wall invertase (INV) (Riesmeier et al., 1994; Eom et al., 2015). Subsequent cleavage of sucrose in starch biosynthesis is mediated by sucrose synthase (SUS) and INVs (Tetlow and Emes, 2019; Braun et al., 2014). SUS hydrolyzes UDP and sucrose to UDP-glucose (UDP-Glc) and fructose (Karrer and Rodriguez, 1992), with UDP-Glc being further converted to glucose-1-phosphate (Glc-1-P) by UDP-Glc pyrophosphorylase (UGP) (Long et al., 2017). INV converts sucrose to fructose and glucose (Chourey et al., 2006), which are further converted into Glc-1-P through a series of enzyme-catalyzed reactions (Kumar et al., 2018). The resulting Glc-1-P is then catalyzed by ADP-glucose (ADP-Glc) pyrophosphorylase (AGP) to form ADP-Glc (Lee et al., 2007), which serves as the glucosyl unit donor for the growing starch polymers (Okita, 1992; Börnke and Sonnewald, 2011).

Similar to seeds, pollen grains are also heterotrophic organs, which are symplastically isolated from the surrounding somatic cell layers. Unlike the sporophytically controlled exine formation, it has long been suggested that intine development and pollen starch accumulation are mainly contributed by gametophytic parts (Shi et al., 2015; Lee et al., 2016). However, few genes involved in starch metabolism of developing pollen have been identified and the mechanism by which pollen starch accumulates remains largely unknown. The RNA-interference (RNAi) plants of *OsINV4* show disruption in pollen starch formation (Oliver et al., 2005). *OsUGP2* mRNA is spatially and temporally found in binucleate microspores and mature pollen (Mu et al., 2009). Downregulation of this gene results in failed accumulation of starch in pollen, thus leading to male sterility (Mu et al., 2009). *RA68* is a gene expressed preferentially in shoots and flowers with unknown function; *RA68*

[1]State Key Laboratory of Crop Gene Exploration and Utilization in Southwest China, Sichuan Agricultural University, Chengdu 611130, China. [2]State Key Laboratory of Hybrid Rice, Rice Research Institute, Sichuan Agricultural University, Chengdu 611130, China.
*These authors contributed equally to this work

‡Authors for correspondence (liping6575@163.com; lisc926105@163.com)

Z.H., 0000-0002-9106-0732; T.Z., 0000-0002-6442-4895; Q.X., 0000-0003-1240-2659; G.Y., 0000-0003-0251-0007; M.L., 0000-0002-6861-5576; Y.T., 0000-0002-0961-9542; D.Z., 0000-0003-0426-0339; X.Z., 0000-0002-9536-8689; S.W., 0000-0003-3163-2476; Y.L., 0000-0002-7427-1028; A.W., 0000-0002-2985-5796; L.W., 0000-0003-3654-1434; S.L., 0000-0001-5684-0533

Handling Editor: Ykä Helariutta
Received 30 August 2020; Accepted 22 February 2021

Development (2021) 148, dev196378. doi:10.1242/dev.196378

knockdown plants show a reduction in pollen viability due to severely defective starch accumulation (Li et al., 2010). A homozygous mutation of the rice *hexokinase 5* gene (*OsHXK5*) leads to significantly reduced pollen starch content (Lee et al., 2019). Phosphoglucomutase (PGM) catalyzes the reversible conversion between Glc-1-P and glucose-6-phosphate (Esposito et al., 1999). The expression of the rice *plastidic PGM* (*OspPGM*) is upregulated in maturing pollen when starch accumulation begins, and the pollen grains of the *osppgm* mutant displayed a starch-null phenotype (Lee et al., 2016).

The L-LecRLKs are a subfamily of RLKs with an intracellular serine/threonine kinase domain, a transmembrane domain and an extracellular legume-like lectin domain (Barre et al., 2002). Recent studies have suggested that L-LecRLKs are involved in plant-pathogen interactions, the stress response and plant development (Vaid et al., 2013; Bellande et al., 2017). In this study, we discovered a novel role for AP1, an L-LecRLK, in starch accumulation during pollen maturation. A mutation in *AP1* caused decreased pollen starch accumulation, altered expressions of numerous genes and downregulated phosphorylation of several proteins involved in the starch and sucrose metabolism pathway in maturing pollen. In addition, our data suggest that AP1 directly interacts with and phosphorylates OsUGP2 to increase its enzymatic activity for pollen starch accumulation. Our work thus enhances the current understanding of the molecular basis of the L-LecRLKs functions and rice pollen starch metabolism.

RESULTS

Isolation of *ap1*

By screening the mutant library, we identified a male-sterile mutant, namely *ap1*. During the vegetative stages of development, the *ap1* mutant showed no obvious difference from the wild-type 9311 (an *indica* rice cultivar; WT) (Fig. 1A). At the heading stage, the flower morphology of the WT and *ap1* were comparable (Fig. 1B,C); however, the mutant had slightly smaller and pale-yellow anthers compared with that of WT (Fig. 1D). By fluorescein diacetate (FDA) staining, we found that the *ap1* pollen grains had an abnormal shape and could not be stained (Fig. 1E-H), indicating that the mutant pollen grains were not viable. I_2-KI staining indicated that the mutant pollen grains contained no starch (Fig. 1I,J). Moreover, viewing the pollen grains under high magnification showed that the mutant pollen grains were almost hollow and lacked typical inclusions (Fig. 1K,L). These findings indicated that the *ap1* mutant is male sterile.

Identification of *AP1*

For the genetic analysis, we pollinated *ap1* with WT pollen grains. The resulting F_1 plants were fertile; and the derived F_2 progeny displayed a nearly 3:1 ratio of fertile and sterile plants (Table S1), indicating that the male-sterile phenotype of *ap1* is controlled by a single recessive locus. Next, we used the MutMap method to map this locus (Abe et al., 2012). By analyzing the re-sequencing data of the mutant, we found a candidate region on the long arm of chromosome 2 harboring a cluster of single nucleotide polymorphisms (SNPs) with index of 1 (Fig. 2A, Fig. S1, Table S2). A SNP occurred in *LOC_Os02g26160* (C1759T) that introduced a stop codon (Fig. 2B), which caused premature translational termination after the 587th residue (Fig. S2). Our further genotypic analysis of the F_2 individuals showed that all the male-sterile plants (Fig. 2C, bottom) had this homozygous mutation (Fig. 2C, top), while the plants with normal fertility (Fig. 2C, bottom) were heterozygous or homozygous for the WT genotype (Fig. 2C top). Besides, this mutation was also segregated with a ratio of 1:2:1 in the F_2 population (Table S1). These results suggested that *LOC_Os02g26160* might be the causal gene of *ap1*.

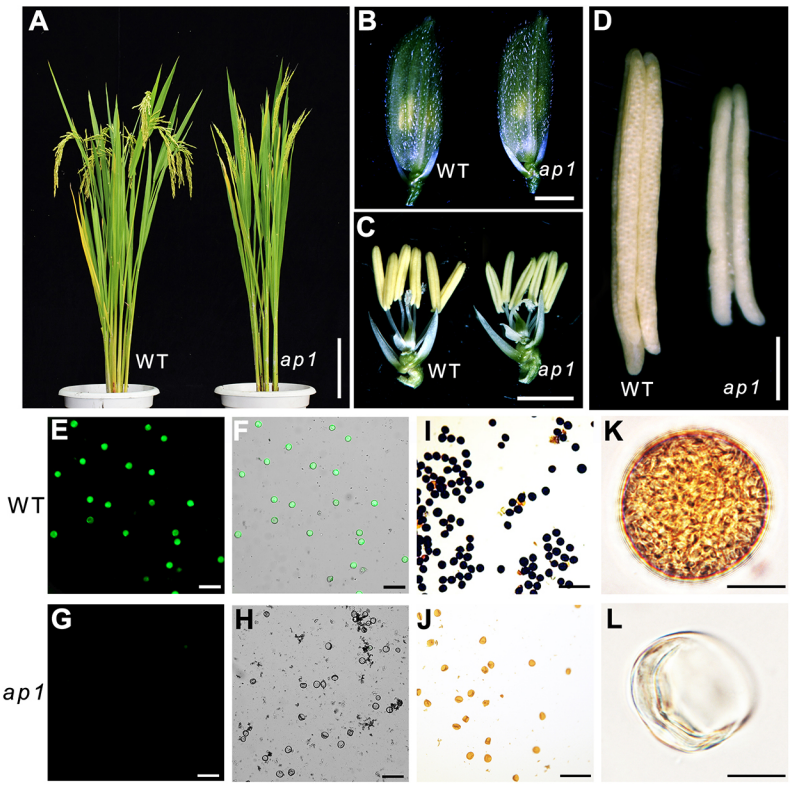

Fig. 1. *ap1* produced sterile pollen grains. (A) Mature plants of the WT and *ap1*. (B) Spikelets of the WT and *ap1* at heading stage. (C) Spikelets of the WT and *ap1* at heading stage after removal of palea and lemma. (D) Anther of the WT and *ap1*. (E-H) FDA staining of pollen grains in the WT (E,F) and *ap1* (G,H). (I,J) I_2-KI solution staining of pollen grains in the WT (I) and *ap1* (J). (K) Pollen grains of the WT showing accumulation of storage materials. (L) Pollen grains of *ap1* showing absence of cytoplasmic contents. Scale bars: 15 cm (A); 2 mm (B,C); 400 µm (D); 200 µm (E-J); 25 µm (K,L).

Development (2021) 148, dev196378. doi:10.1242/dev.196378

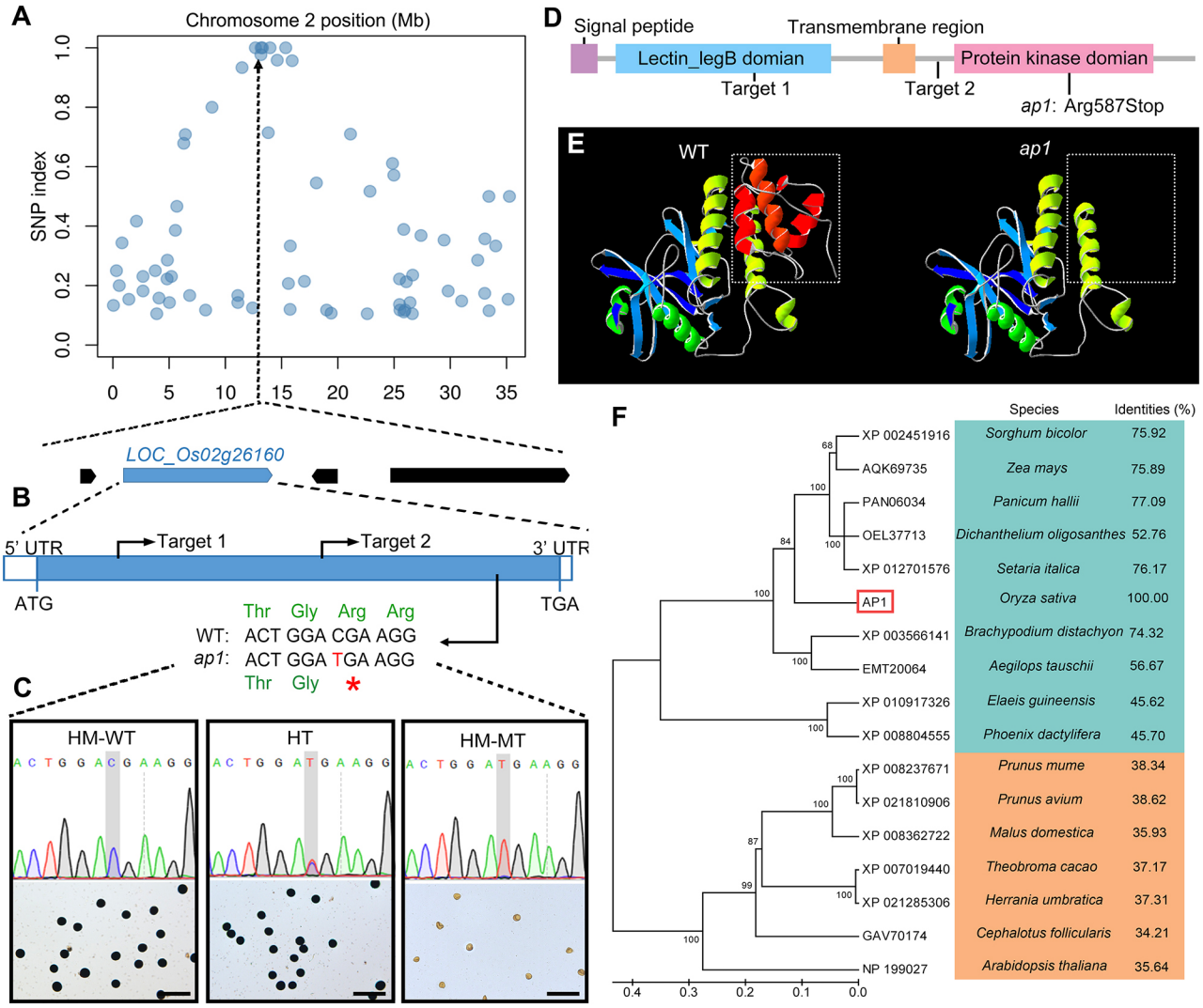

Fig. 2. Molecular identification of *AP1*. (A) Distributions of the SNP index on chromosome 2. The arrow indicates the candidate mutation site. (B) Gene model of *LOC_Os02g26160* (*AP1*). The arrows indicate the CRISPR/Cas9 target sites or the *ap1* mutation site. Blue box, exon; white boxes, untranslated regions (UTRs). (C) Co-segregation analysis of the *ap1* mutation and the male-sterile phenotype. HM-WT, HT and HM-MT indicate the homozygous WT genotype, heterozygous genotype and homozygous mutant genotype, respectively. (D) Schematic diagram of AP1 protein structure. Purple box, signal peptides; blue box, lectin_legB domain (Pfam ID: PF00139); orange box, transmembrane region; pink box, protein kinase domain (Pfam ID: PF00069). (E) Predicted model of AP1 protein in the WT and *ap1*. The three-dimensional protein structures were predicted using SWISS-MODEL (http://swissmodel.expasy.org) with the same template. (F) A phylogenetic tree of AP1-related proteins. The protein accession numbers in GenBank are shown. Monocots and dicots are in blue and orange backgrounds, respectively. The numbers on the right represent the percentage identities between AP1 and its ortholog in corresponding species. The tree was constructed based on the results of multiple protein alignments in Fig. S3. Scale bars: 200 µm.

LOC_Os02g26160 encodes a putative L-LecRLK (Vaid et al., 2012), which contains a N-terminal signal peptide, a Lectin_legB domain (Pfam: PF00139), a transmembrane region and a protein kinase (PK) domain (Pfam: PF00069) (Fig. 2D). Modeling of protein tertiary structure indicated that the *ap1* mutation resulted in the absence of three α-helixes of the PK domain and the C terminus (Fig. 2E), suggesting this mutation might impair protein function. Phylogenetic analysis showed that, although this L-LecRLK protein is more closely related to its monocot orthologs, it constitutes an isolated branch (Fig. 2F, Fig. S3), suggesting a potential functional diversification between this L-LecRLK protein and its homologs in other plant species.

Functional validation of *AP1*

To conduct a functional analysis, we designed two independent targets (Fig. 2B,D) and used the CRISPR/Cas9 method to knockout *LOC_Os02g26160* in Nipponbare (a *japonica* rice cultivar) plants. Sequencing analysis identified five CRISPR/Cas9-mediated (*cr*) mutants with different types of homozygous mutations (Fig. 3A). An analysis of amino acids showed that all these mutations led to frame shifts, which in turn caused the pre-termination of protein translation (Fig. 3A, Fig. S4), suggesting the disruptions of *LOC_Os02g26160* function within these mutants. Notably, two *cr* mutant lines (*cr-2-3* and *cr-2-11*) (Fig. 3A) generated from editing of Target 2 lacked the C-terminal PK domain (Fig. 3B), similar to that of *ap1*. The following phenotypic observations revealed that, compared with Nipponbare, all of these *cr* mutants had yellow-white anthers (Fig. 3C) and produced hollow pollen grains (Fig. 3D) but displayed normal vegetative growth and flower morphology (Fig. S5A,B), mimicking the phenotypes of *ap1*.

Additionally, we performed a functional complementation analysis by transforming a Nipponbare genomic fragment – which

Development (2021) 148, dev196378. doi:10.1242/dev.196378

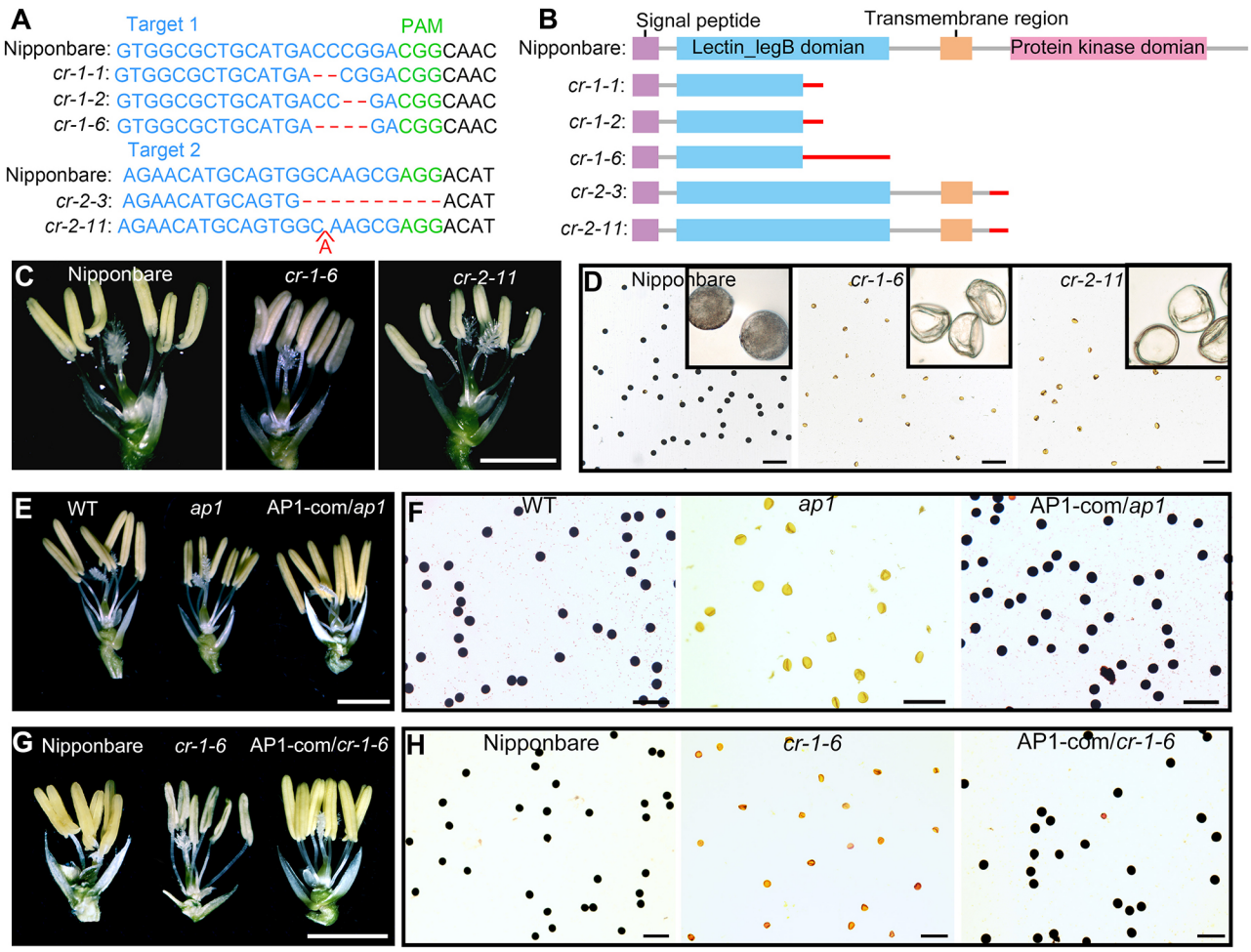

Fig. 3. Functional analysis of AP1. (A) Mutation analysis of the CRISPR/Cas9-mediated (*cr*) mutants. (B) Schematic diagrams of the truncated AP1 proteins in the *cr* mutants. (C) Spikelets of Nipponbare and the *cr* mutants at heading stage after removal of palea and lemma. (D) I_2-KI solution staining of pollen grains in Nipponbare and the *cr* mutants. (E) Spikelets of the WT, *ap1* and the complemented line (AP1-com/*ap1*) at heading stage after removal of palea and lemma. (F) I_2-KI solution staining of pollen grains in the WT, *ap1* mutant and the complemented line (AP1-com/*ap1*). (G) Spikelets of Nipponbare, the *cr* mutant and the complemented line (AP1-com/*cr-1-6*) at heading stage after removal of palea and lemma. (H) I_2-KI solution staining of pollen grains in Nipponbare, the *cr* mutant and the complemented line (AP1-com/*cr-1-6*). Scale bars: 2 mm (C,E,G); 200 µm (D,F,H).

included a ~2 kb promoter region, 2 kb coding region and 0.8 kb 3′ UTR of *LOC_Os02g26160* – into the *ap1* and *cr* mutants. The positive transgenic plants all showed rescue of the male-sterile phenotype of both the *ap1* (Fig. 3E,F) and *cr* (Fig. 3G,H) homozygous plants. These results confirmed that the male-sterile phenotype in the mutants is indeed caused by dysfunction of *LOC_Os02g26160/AP1*, indicating a crucial role of *AP1* in the development of male gametes.

Expression pattern of *AP1*

Quantitative real-time PCR (qRT-PCR) analysis revealed that *AP1* was mainly expressed in spikelets with developing anthers and roots (Fig. 4A). Interestingly, *AP1* expression gradually increased with anther development and reached its first peak in spikelets with anthers at stage 8 or 9, and then decreased but rapidly increased again to its maximum level in spikelets at stage 11 or 12. GUS activity in transgenic plants with the GUS reporter gene driven by the native promoter of *AP1* also showed this expression pattern (Fig. 4B). Importantly, GUS staining also revealed a high accumulation of *AP1* transcripts in the anthers at stage 11 (Fig. 4C), especially in microspores (Fig. 4D), which was further confirmed by RNA *in situ* hybridization (Fig. 4E,F).

Using the WoLF PSORT program (https://wolfpsort.hgc.jp/), AP1 was predicted as a plasma membrane-localized protein. The C-terminal PK domain of AP1 is likely intracellularly located (Fig. S6) (TMHMM 2.0 program, http://www.cbs.dtu.dk/services/TMHMM/). As expected, transient expression of an AP1-YFP fusion protein construct (Fig. 4G) in rice protoplasts (Fig. 4H-L) and *Nicotiana benthamiana* (tobacco) leaf epidermal cells (Fig. 4M-P) showed that AP1-YFP was well overlapped with the signals of a plasma membrane marker (OsPIP2.1-mCherry) (Dangol et al., 2017), indicating this protein was exclusively targeted to the plasma membrane. These results established that AP1 is a plasma membrane protein that is primarily located in microspores.

Cellular defects of anther and pollen development in *ap1*

To detect possible cellular defects of anther and pollen development in *ap1*, we examined the chromosome behaviors of WT and *ap1* PMCs during the meiotic process by 4′,6-diamidino-2-phenylindole (DAPI) staining. The results showed that the mutant meiotic cells had a WT-like chromosome synapsis and condensation, as well as cytokinesis (Fig. S7A), suggesting that the mutation of *AP1* might not affect the meiotic process. Using Aniline Blue staining, we also observed similar callose signals of tetrads in the WT and the mutant (Fig. S7B).

Development (2021) 148, dev196378. doi:10.1242/dev.196378

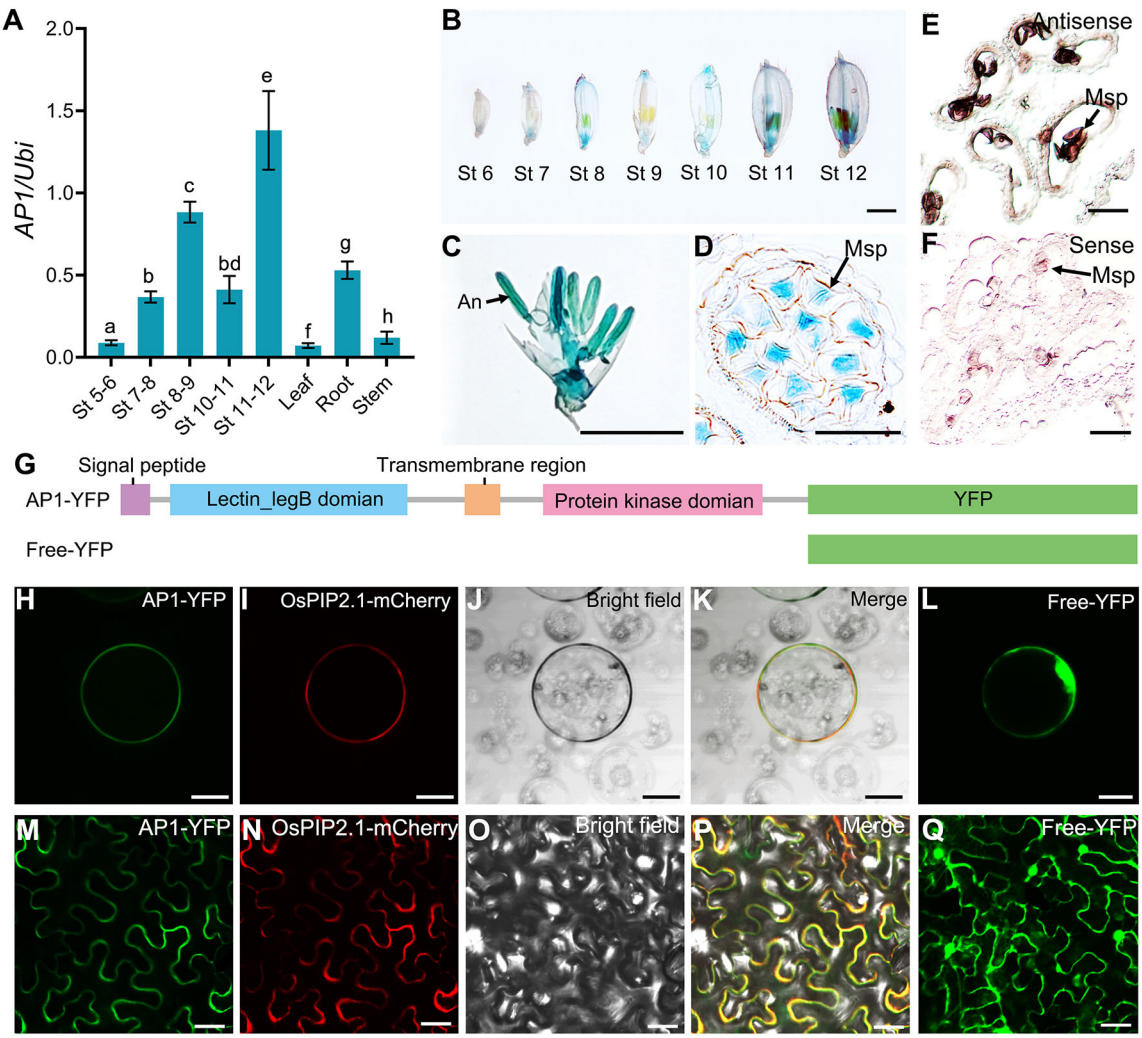

Fig. 4. Expression analysis of *AP1*. (A) qRT-PCR analysis of *AP1*. RNAs were extracted from spikelets with anthers at different development stages. Data are mean±s.e.m. of four biological replicates. Statistical significance was determined by one-way ANOVA; significant differences (P<0.05) are indicated by different lowercase letters. (B-D) GUS activity in $AP1_{pro}$::*GUS* transgenic line. (B) GUS activity in spikelets with anthers at different development stage. (C) GUS activity in spikelets with anthers at stage 11. Lemma and palea were removed. (D) Section of anther in C. (E,F) RNA *in situ* hybridization in anthers at stage 11. Probed with the *AP1* antisense probe (E) and sense probe (F). (G) A schematic diagram of the constructs used for subcellular localization. (H-K) Subcellular localization of AP1 in rice protoplast. The fusion proteins (AP1-YFP) (H) were co-expressed with the plasma membrane marker (OsPIP2.1-mCherry) (I). (L) Subcellular localization of the control (free-YFP) in rice protoplast. (M-P) Subcellular localization of AP1 in tobacco leaf epidermis cells. The fusion proteins (AP1-YFP) (M) were co-expressed with the plasma membrane marker (OsPIP2.1-mCherry) (N). (Q) Subcellular localization of the control (free-YFP) in tobacco leaf epidermis cells. An, anther; Msp, microspore; St, stage. Scale bars: 2 mm (B,C); 40 µm (D-F); 10 µm (H-L); 25 µm (M-Q).

We compared the cross-sections of developing anthers in the WT and *ap1* according to the stages divided by Zhang and Wilson (2009). From stages 8a to 9, PMCs of both the WT and the mutant underwent meiosis normally (Fig. 5A,B,E,F), and then released free haploid microspores from tetrads (Fig. 5C,G), in agreement with our previous observations. Moreover, no significant defects were detected in the mutant anthers until stage 11 (Fig. 5D,H,I,M). At late stage 11, the mutant microspores appeared to have less cytoplasm content (Fig. 5N) compared with that of WT (Fig. 5J). Subsequently, the mutant microspores showed a severely impaired accumulation of storage material (Fig. 5O), which resulted in abnormally hollow and deflated pollen grains in the anther locule (Fig. 5P). In contrast, the WT microspores became maturing and then engorged with cytoplasm and starch granules (Fig. 5K,L).

We used electron microscopy to further understand the ultrastructural defects in *ap1*. The transmission electron microscope (TEM) results revealed that the mutant microspores vacuolated normally and thereafter formed a sickle shape with the complete deposition of the double-layered exine during stage 10 to early stage 11 (Fig. 6E-H), resembling the WT (Fig. 6A-D). At late stage 11, the WT microspores had a normal pollen wall, consisting of the exine and intine layers, and began to accumulate starch in the cytoplasm (Fig. 6I-K). However, the mutant microspores neither formed any intine-like structures nor showed signs of inclusion storage (Fig. 6L-N). At stage 12, the spherical WT pollen grains were fully packed with inclusions, such as starch granules (Fig. 6O-Q). In contrast, the cytoplasm of the mutant microspores degraded further, leaving an empty cellular space inside a shrunken exine layer (Fig. 6S-U). These results were consistent with the light microscope observations.

In addition, we found that, although the inner Ubisch bodies and the outer cuticle of the mutant anther wall (Fig. 6U,V) appeared to have developed normally, the arrangements of these two structures were denser than that of the WT (Fig. 6Q,R). Furthermore, we found an abnormally flat aperture in the mutant microspores (Fig. 6T)

Development (2021) 148, dev196378. doi:10.1242/dev.196378

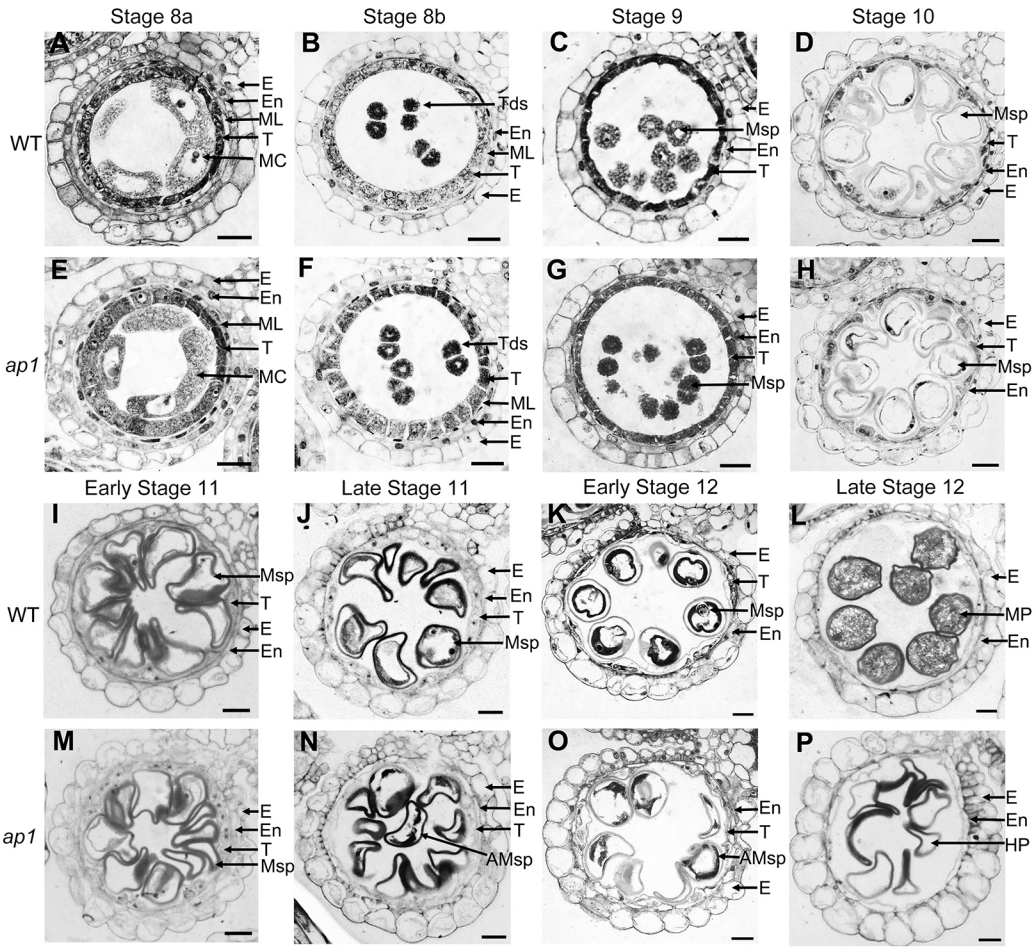

Fig. 5. Transverse section analysis of anther and pollen development in the WT and *ap1*. (A-D,I-L) Transverse sections of the WT anthers at stages 8a, 8b and 9-12. (E-H,M-P) Transverse sections of *ap1* anthers at stages 8a, 8b and 9-12. AMsp, abnormal microspores; E, epidermis; En, endothecium; HP, hollow pollen; MC, meiotic cell; ML, middle layer; MP, mature pollen; Msp, microspore; T, tapetum; Tds, tetrads. Scale bars: 15 µm.

compared with the thick annulus surrounding the aperture of WT microspores (Fig. 6B). In support of these observations, further scanning electron microscope (SEM) analysis of the stage 12 anthers was carried out. The results showed that, compared with the WT (Fig. S8A-D,I-L), *ap1* displayed thinner anthers (Fig. S8E) with more tightly distributed cuticular ridges (Fig. S8F,G) and Ubisch bodies (Fig. S8H), as well as pollen grains that lacked the annulus structure around the aperture (Fig. S8M-P). We also examined the cellular features of developing anthers and the surface of mature pollen in the *cr* mutants using cross-sections and SEM analysis, respectively. The results showed that the *cr* mutants also exhibited deficient engorgement of pollen storage materials (Fig. S9) and abnormal annulus of the pollen aperture (Fig. S10), which were identical to the defects observed in *ap1*. These findings demonstrated that dysfunction of *AP1* not only caused the defective accumulation of pollen storage materials, but also affected the formation of the intine and aperture during pollen development.

The starch and sucrose metabolism process is disturbed in *ap1* pollen

To further explore the roles of AP1 in the late stages of pollen development, a transcriptome analysis of spikelets with anthers during stages 11 to 12 from the WT and *ap1* plants was conducted. RNA-seq data showed that the *ap1* mutation resulted in thousands of differentially expressed genes (DEGs), including 1221 downregulated and 936 upregulated transcripts (Fig. 7A). A Kyoto Encyclopedia of Genes and Genomes (KEGG) pathway analysis revealed that these DEGs were assigned into several functional classes. Among these classes, the biological processes of starch and sucrose metabolism were significantly enriched (Fig. 7B). In this class, a number of genes putatively related to sugar signaling and conversion, such as *LOC_Os01g69030* (*sucrose-phosphate synthase*, *SPS*), *LOC_Os06g14510* (*sugar isomerase*, *SIS*), *LOC_Os03g53790* (*periplasmic β-glucosidase*, *PBGlu*), *OsHXK7* (*cytosolic hexokinase*) (Kim et al., 2016), *Os9bglu30* (*β-glucosidase*) and *LOC_Os06g46340* (*glycosyl hydrolase*, *GH*) were downregulated in *ap1* (Fig. 7C). The identical reduction in transcript level of these genes in *ap1* and the *cr* mutants was also validated by our further qRT-PCR data (Fig. 7D, Fig. S11). Considering the close connection between sugar metabolism and starch biosynthesis (Chourey et al., 1998; Braun et al., 2014), these results implied a disordered sugars metabolism that may result in the deficiency of starch biosynthesis in *ap1*.

Starch is one of the main components in pollen storage materials and is necessary for pollen viability (Datta et al., 2001). We therefore determined the starch content in anthers from the WT and *ap1* plants during pollen maturation. In agreement with the observed defects of pollen inclusion storage in *ap1* (Fig. 1I-L), the mutant showed significantly decreased levels of starch at the late pollen development

Development (2021) 148, dev196378. doi:10.1242/dev.196378

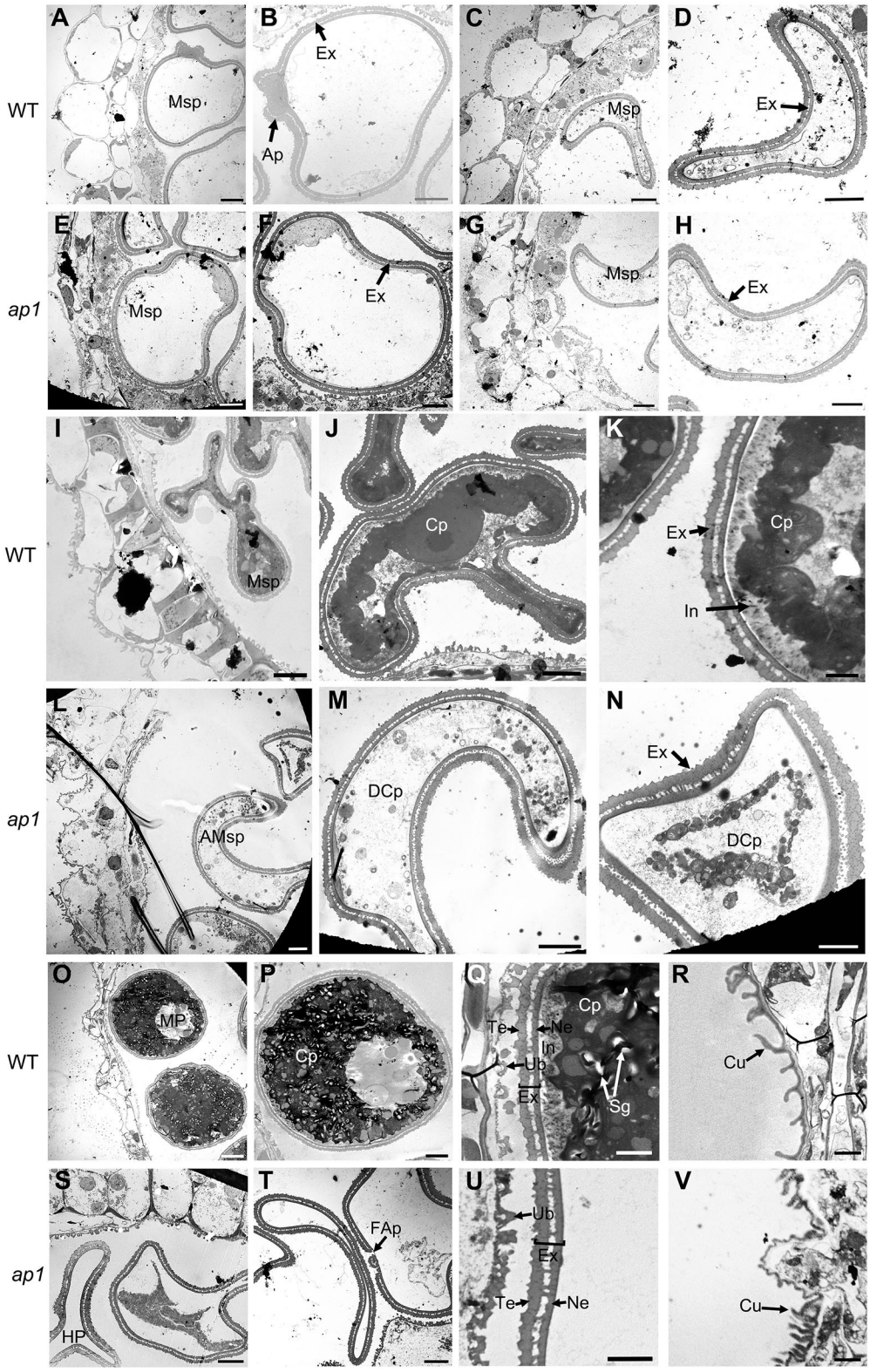

Fig. 6. TEM analysis of anther and pollen development in the WT and *ap1*. (A-D,I-K,O-R) TEM analysis of anther and pollen development in the WT. (E-H,L-N,S-V) TEM analysis of anther and pollen development in *ap1*. (A,E) Anther at stage 10. (B,F) Microspore at stage 10. (C,G) Anther at stage 11. (D,H) Microspore at stage 11. (I,L) Anther at late stage 11. (J,M) Microspore at late stage 11. (K,N) Detailed images of microspore at late stage 11. (O,S) Anther at stage 12. (P,T) Pollen at stage 12. (Q,U) Ubisch bodies and pollen wall at stage 12. (R,V) Anther cuticle layer at stage 12. AMsp, abnormal microspores; Ap, aperture with annulus; Cp, cytoplasm; Cu, cuticle; DCp, degrading cytoplasm; Ex, exine; FAp, flat aperture lacking annulus; HP, hollow pollen; In, intine; MP, mature pollen; Msp, microspore; Ne, nexine; Sg, starch grain; Te, tectum; Ub, Ubisch body. Scale bars: 10 µm (A,C,E,G,I,L,O,S); 5 µm (B,D,F,H,J,M,P,T); 2 µm (K,N,Q,R,U,V).

stages compared with that of the WT (Fig. 7E). These results supported that AP1 may participate in pollen starch accumulation.

The phosphorylation level of OsUGP2 was downregulated in *ap1*

To verify the kinase activity of AP1, we fused the C-terminal PK domain of AP1 with glutathione S-transferase (GST; GST-AP1-C) and performed an *in vitro* kinase assay. The results showed that the GST-AP1-C incubated with phosphorylation buffer (PB) has a significantly stronger phosphorylation level than that of the unincubated GST-AP1-C (Fig. 8A, Fig. S12), supporting that AP1 has kinase activity and can be auto-phosphorylated.

To gain insight into the putative downstream members of AP1 in the accumulation of pollen storage materials, we used a

Development (2021) 148, dev196378. doi:10.1242/dev.196378

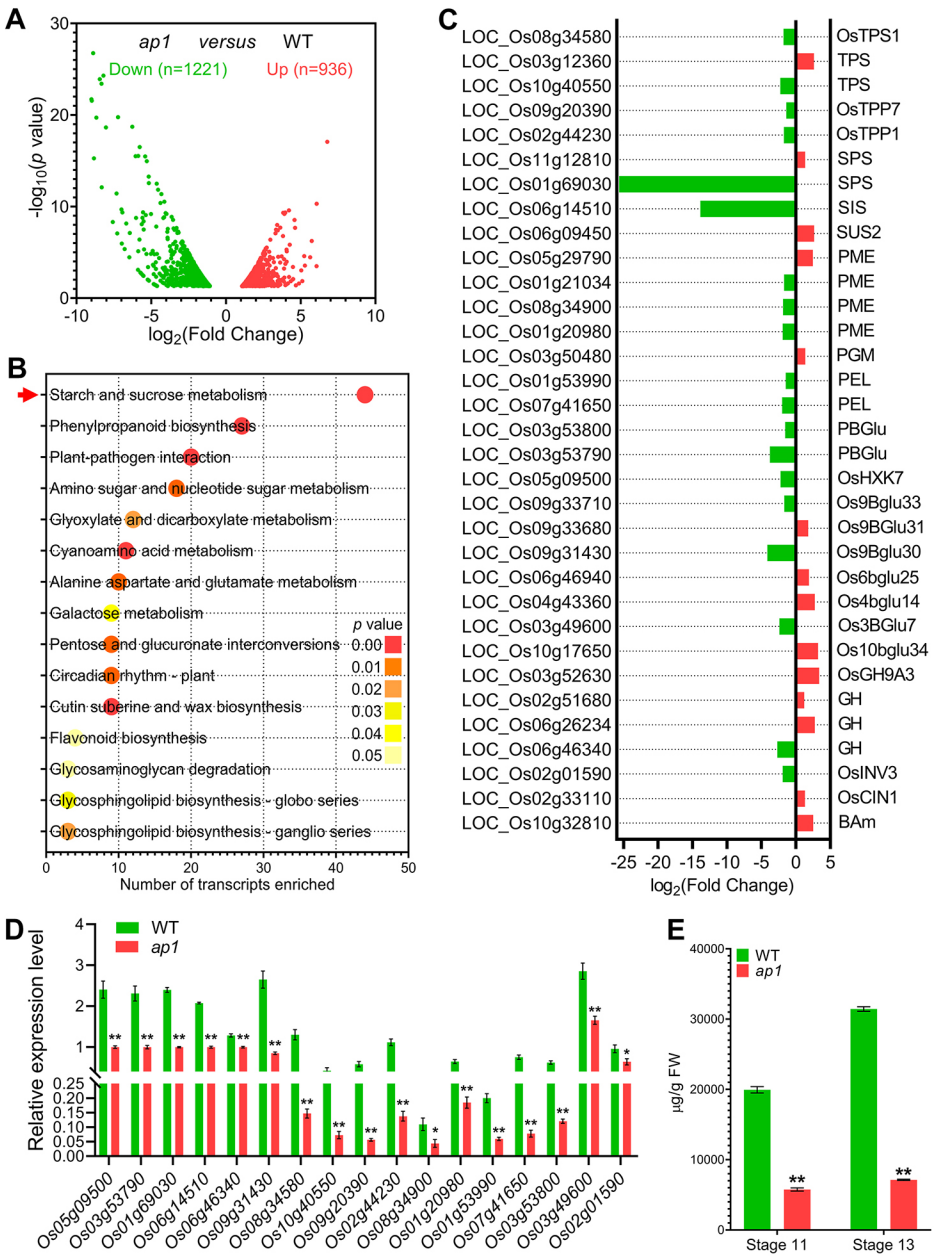

Fig. 7. Impact of the *ap1* mutation on starch metabolism and genes expression. (A) The volcano plot of different expressed transcripts (statistical significance $P<0.05$) between the WT and *ap1* revealed by RNA-seq. Two biological replicates were used. (B) KEGG analysis of the DEGs. Categories with statistical significance ($P<0.05$) are shown. (C) The DEGs involved in starch and sucrose metabolism. (D) qRT-PCR validation of several starch and sucrose metabolism-related genes in C. Spikelets of the WT and the *ap1* mutants with anthers during stage 11 to 12 were used for RNA extraction. Data are mean±s.e.m. of four biological replicates (*$P<0.05$ and **$P<0.01$ compared with the WT using an unpaired two-tailed Student's *t*-test). (E) Starch content of the WT and *ap1* anthers. Data are mean±s.d. (**$P<0.01$ compared with the WT using an unpaired two-tailed Student's *t*-test). BAm, β-amylase; CIN, cell wall invertase; GH, glycosyl hydrolase; INV, vacuolar acid invertase; PBGlu, periplasmic β-glucosidase; PEL, pectate lyase; PGM, phosphoglucomutase; PME, pectin methylesterase; PMEI, pectin methylesterase inhibitor; SIS, sugar isomerase; SPS, sucrose-phosphate synthase; SUS, sucrose synthase; TPP, trehalose-6-phosphate phosphatase; TPS, trehalose-6-phosphate synthase.

quantitative phosphoproteomic approach to investigate its potential *in vivo* targets. We analyzed the anther samples from WT and *ap1* plants during stages 11 to 12. This analysis identified that a total of 2246 unique phosphorylation sites from 1449 proteins showed >1.5-fold difference ($P<0.05$) between WT and *ap1* (see Table S5), of which 940 phosphoproteins were downregulated and 509 proteins were upregulated in the mutant (Fig. 8B). As AP1 is an active kinase, we assumed that its targets would reduce the phosphorylation level in the mutant plants. We then focused on the downregulated phosphoproteins. The KEGG pathway analysis indicated that the downregulated phosphoproteins were enriched in serval pathways (Fig. 8C). Consistent with the defective starch accumulation in *ap1* pollen grains, key enzymes involved in the starch and sucrose metabolic pathway, such as OsHXK5 in sugar cleavage, and OsUGP2 and PGMs in Glc-1-P production, were also significantly enriched (Fig. 8C and Table S3). Further investigation showed that the phosphorylation levels of OsUGP2 were apparently decreased at two serine residues (S151 and S413; Fig. 8D, Fig. S13, Table S3). To exclude the possibility that the downregulation of OsUGP2 phosphorylation is correlated with its mRNA transcript level, we quantified the expression level of *OsUGP2* and detected no significant differences between the WT and *ap1* mutant (Fig. S14A), suggesting this was a direct consequence of the loss of AP1 phosphorylation function. Similar to *AP1* (Fig. 4A-F), *OsUGP2* is highly expressed in the spikelets with anthers at stages 11 to 12 (Fig. S14B), and its protein is also predominately located in maturing pollen grains (Mu et al., 2009). Moreover, the phenotype of *ap1* (Figs 1 and 5) is similar to that of the *OsUGP2* knockdown plants (Mu et al., 2009). Considering these similarities and the important role of OsUGP2 in starch accumulation during rice pollen maturation (Mu et al., 2009), we speculated that OsUGP2 is a potential candidate for AP1 substrates.

Development (2021) 148, dev196378. doi:10.1242/dev.196378

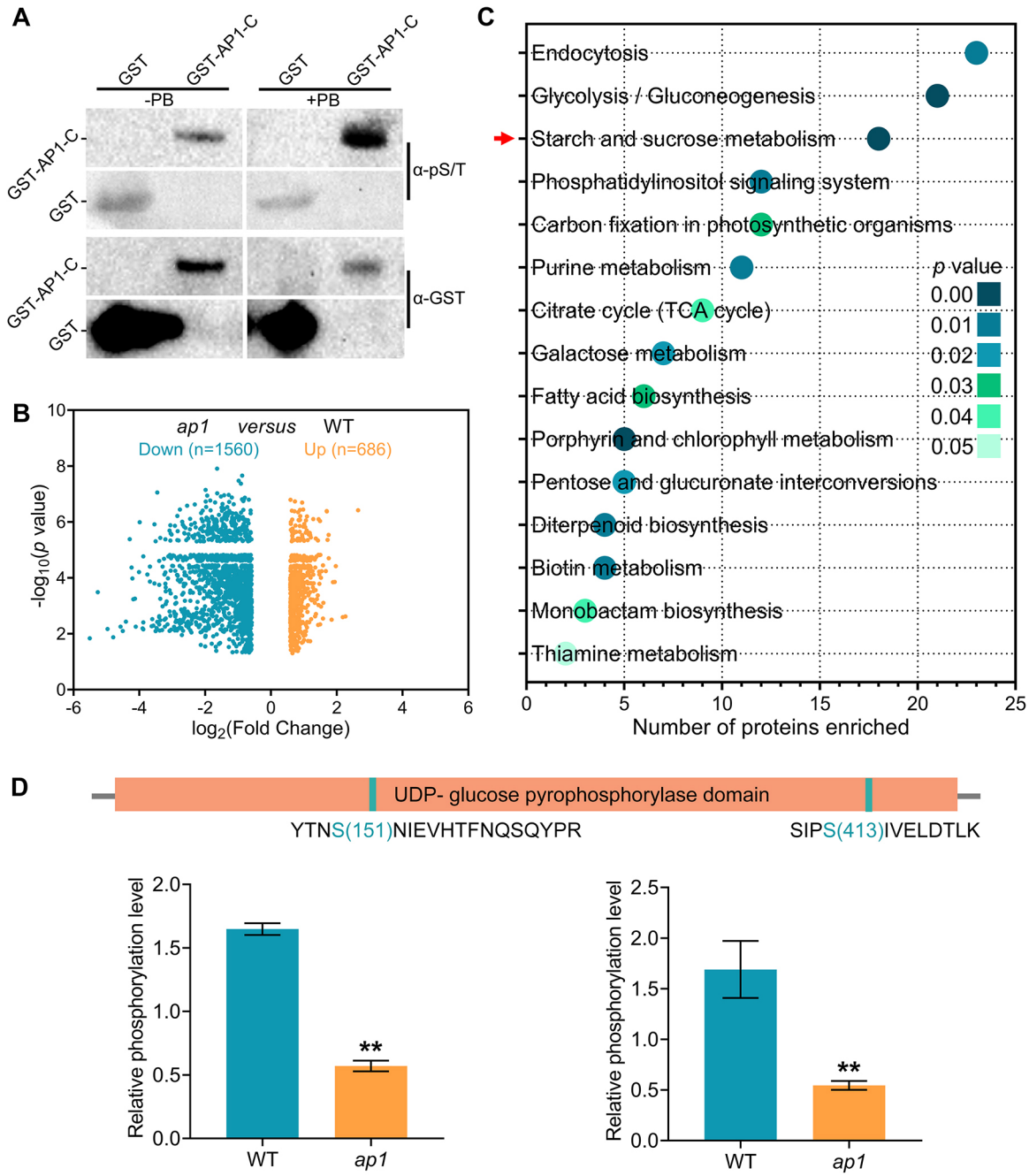

Fig. 8. Comparative phosphoproteomic analysis of the WT and *ap1* anthers. (A) Auto-phosphorylation analysis of AP1. α-pS/T, anti-phospho (Ser/Thr) Phe antibody; α-GST, anti-GST antibody; PB, phosphorylation buffer. (B) The counts of down- and upregulated phosphorylation sites, which showed >1.5-fold difference (statistical significance $P<0.05$) between the WT and *ap1*. (C) KEGG analysis of downregulated phosphoproteins. Categories with statistical significance ($P<0.05$) are shown. (D) Schematic diagram of the downregulated phosphorylation sites in OsUGP2 (upper) and relative phosphorylation level of each site (lower). Orange box, UDP-glucose pyrophosphorylase domain (Pfam ID: PF01704). Data are mean±s.d. of three biological replicates. $^{**}P<0.01$ compared with the WT using an unpaired two-tailed Student's *t*-test.

AP1 directly interacts with OsUGP2

Previous studies have reported that plant PKs typically phosphorylate their substrates by physical interactions to modulate developmental and biosynthetic processes (Mao et al., 2011; Tian et al., 2017). It is worth noting that, apart from the downregulated phosphorylation of OsUGP2 in the *ap1* mutant, *OsUGP2* and *AP1* are co-expressed at the stage of pollen starch accumulation (Fig. 4A-F, Fig. S14B) (Mu et al., 2009). The subcellular localization assay also showed the overlapped distributions of co-expressed AP1-YFP and OsUGP2-CFP (Fig. S15). Therefore, we used a yeast two-hybrid (Y2H) assay to determine whether AP1 could interact with OsUGP2 directly. Indeed, the results of the Y2H assay revealed a positive interaction between the AP1-C and OsUGP2 in yeast cells (Fig. 9A).

To validate the interaction of AP1 with OsUGP2, we conducted the bimolecular fluorescent complementary (BiFC) assays in tobacco leaves. We found that both full-length AP1 protein and AP1-C were able to interact with OsUGP2 in tobacco leaf epidermal cells

Development (2021) 148, dev196378. doi:10.1242/dev.196378

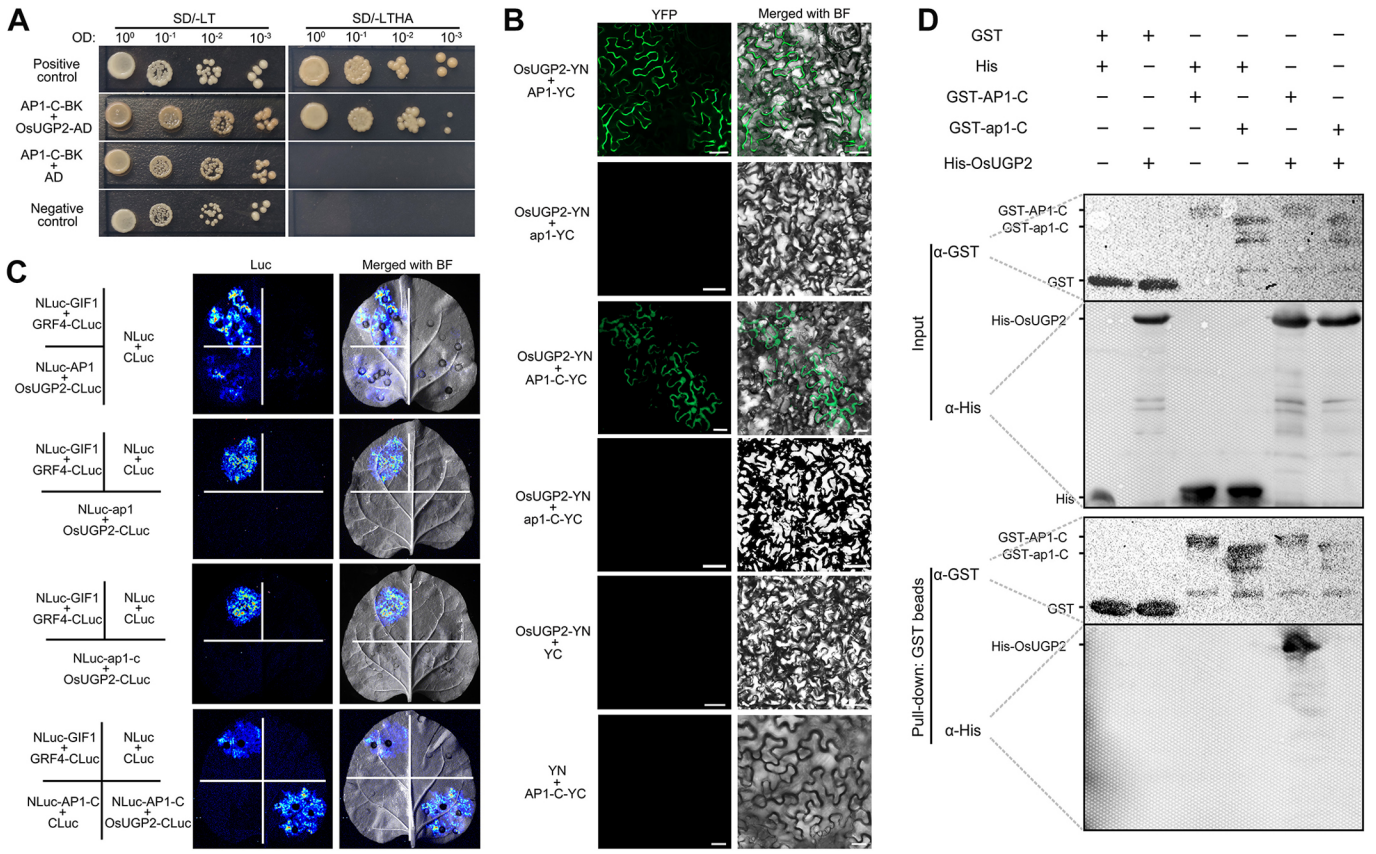

Fig. 9. AP1 interacts with OsUGP2. (A) The Y2H assay. pGBKT7-Murine p53 and pGADT7-SV40 large T-antigen were set as the positive control pair. pGBKT7-Lamin and pGADT7-SV40 large T-antigen were set as the negative control pair. SD/−LT, synthetic dropout medium lacking leucine and tryptophan; SD/−LTHA, synthetic dropout medium lacking leucine, tryptophan, histidine and adenine. (B) The BiFC assay in tobacco leaf epidermis cells. (C) The LCI assay in tobacco leaf epidermis cells. NLuc-GIF1 and GRF4-CLuc are positive controls. NLuc and CLuc are the negative controls. (D) The GST pull-down assay. Purified recombinant proteins GST-AP1-C, GST-ap1-C (mutated version) or GST were incubated with His-OsUGP2 or His followed by GST-mediated pull-down. Scale bars: 25 µm.

(Fig. 9B). In contrast, no positive interaction was detected between the AP1 mutated protein and OsUGP2 (Fig. 9B), suggesting that the PK domain of AP1 is responsible for mediating AP1-OsUGP2 interactions. Subsequently, we performed a firefly luciferase complementation imaging (LCI) assay in tobacco leaves (Chen et al., 2008). As expected, the co-expression of OsUGP2-CLuc with NLuc-AP1-C or NLuc-AP1 constructs in tobacco leaves also confirmed the interaction between AP1 and OsUGP2 (Fig. 9C). In addition, GST pull-down assays revealed that a complex containing the GST-AP1-C and the His-tagged OsUGP2 protein (His-OsUGP2) formed *in vitro* (Fig. 9D), whereas the His-OsUGP2 protein did not bind to the mutated PK domain of AP1 protein (GST-ap1-C) (Fig. 9D). Taken together, both *in vivo* and *in vitro* results indicated that AP1 directly interacts with OsUGP2 through its PK domain.

Phosphorylation by AP1 increases the enzymatic activity of OsUGP2

The interaction between AP1 and OsUGP2 suggests that OsUGP2 may be a direct phosphorylation target of AP1. In order to investigate whether OsUGP2 can be phosphorylated by AP1, recombinant His-OsUGP2 protein was incubated with GST-AP1-C or GST-ap1-C for a phosphorylation assay. The immunoblotting results showed that the PK domain of AP1 strongly trans-phosphorylated OsUGP2 *in vitro*, whereas the AP1 mutated version of the PK domain lost auto-phosphorylation activity and failed to phosphorylate OsUGP2 (Fig. 10A). In addition, changing both S151 and S413 to alanine (OsUGP2^{AA}) largely impaired the phosphorylation of OsUGP2 by GST-AP1-C (Fig. 10A).

To explore the effects of the phosphorylation of OsUGP2 by AP1, we measured whether the enzymatic activity of His-OsUGP2 changed with the presence of AP1 *in vitro*. As shown in Fig. 10B, when co-incubated with GST-AP1-C, His-OsUGP2 exhibited higher levels of enzymatic activity than did His-OsUGP2 alone and co-incubation of His-OsUGP2 and GST-ap1-C. To test whether the phosphorylation of S151 and S413 is required for OsUGP2 activity, we created another mutated version of OsUGP2, OsUGP2^{DD} (changing both S151 and S413 to aspartic acid), which mimics the phosphorylated S151 and S413. The results showed that, unlike His-OsUGP2, the enzymatic activity of His-OsUGP2^{AA} was lower than that of His-OsUGP2^{DD}, and could not be increased by incubation with GST-AP1-C (Fig. 10B).

To confirm the effects of the S151 and S413 phosphorylation of OsUGP2 in planta cells, we transiently expressed OsUGP2 and its variants in tobacco leaf cells and assessed their effects on starch content. The results showed that cells expressing OsUGP2^{DD} and cells co-expressing AP1 and OsUGP2 had a similar starch content, which was significantly higher than that of OsUGP2 alone and the combination of ap1 and OsUGP2 (Fig. 10C). Cells expression of OsUGP2^{AA} alone had a low starch content as the controls (Fig. 10C). Therefore, our *in vitro* and *in vivo* data suggested that AP1 directly affects OsUGP2 activity to promote starch

Development (2021) 148, dev196378. doi:10.1242/dev.196378

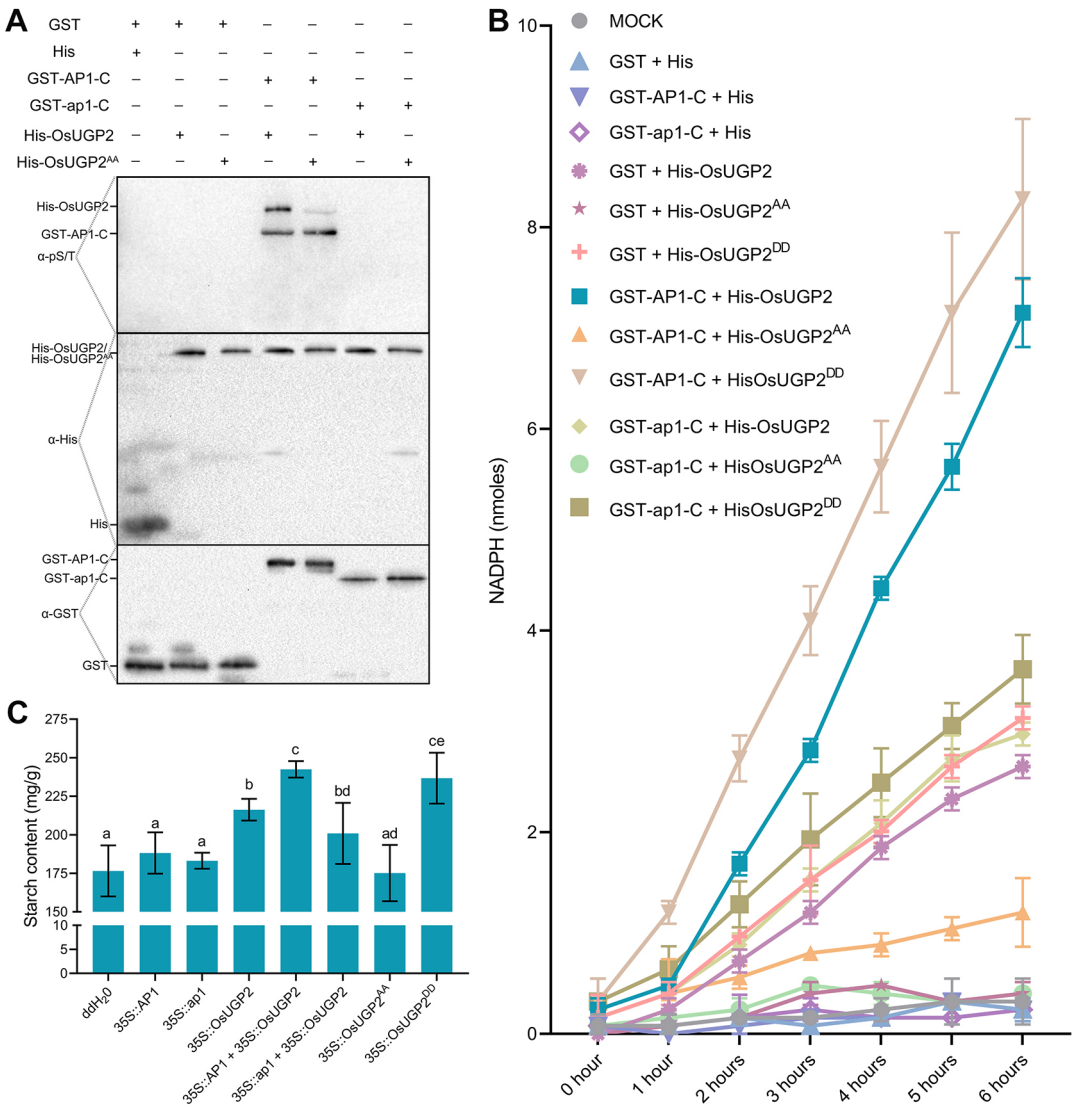

Fig. 10. AP1 phosphorylates OsUGP2 and promotes its enzymatic activity. (A) *In vitro* phosphorylation of OsUGP2 by AP1. The phosphorylated proteins were detected by anti-phospho (Ser/Thr) Phe antibody (α-pS/T) immunoblotting. Protein loading was detected by anti-GST (α-GST) antibody or anti-His (α-His) antibody immunoblotting. (B) AP1 promotes the enzymatic activity of OsUGP2 *in vitro*. The content of NADPH reflects the enzymatic activity of OsUGP2. Data are mean±s.d. of three replicates. (C) Starch content of tobacco leaf cells transiently expressed with different constructs. Tobacco cells injected with double distilled H_2O were used as the control. Data are mean±s.d. of three replicates. Statistical significance was determined by one-way ANOVA; significant differences (P<0.05) are indicated by different lowercase letters.

biosynthesis possibly by post-translational modifications of phosphorylation.

DISCUSSION

Mature pollen grains of rice are usually surrounded by a pollen wall and are typically full of stored carbohydrates such as starch (Feng et al., 2001; Zhang et al., 2011). In rice, previous studies have revealed the factors that contribute to pollen wall formation, such as Acyl-CoA Synthetase12, Polyketide Synthases1/2 and Strictosidine Synthase-like2 for exine formation (Zou et al., 2017a,b, 2018), as well as Collapsed Abnormal Pollen1, ATP Binding Cassette G Transporter3 and Glycosyltransferase1 for intine formation (Moon et al., 2013; Ueda et al., 2013; Luo et al., 2019). However, the underlying mechanism by which storage materials accumulated during pollen maturation remains largely unknown. Here, we presented findings supporting the novel role of AP1, an L-LecRLK, in pollen starch accumulation during pollen maturation in rice.

Morphological observations suggest that loss-of-function of *AP1* resulted in abnormal and nonviable pollen with little or no pollen storage materials (Fig. 1). According to our cytological observations (Figs 5 and 6, Fig. S8), the mutant pollen underwent normal meiosis, haploid microspore release and vacuolation, but showed subcellular abnormality during pollen maturation. The defected accumulation of pollen storage was observed at this stage in the mutant. Starch is the main component of pollen cytoplasm in major cereal crops, its accumulation is required for pollen maturation and it is responsible for pollen viability (Wen and Chase, 1999; Datta et al., 2001). Consistent with this, we observed a significantly lower starch content in the anthers of mutant plants at late developmental stages (Fig. 7E). In addition, the mutant pollen grains also had a deformed aperture and intine (Fig. 6, Fig. S8). It has previously been suggested that pollen starch synthesis and intine formation are mainly controlled by the gametophyte (Shi et al., 2015; Lee et al., 2016). Our results

Development (2021) 148, dev196378. doi:10.1242/dev.196378

provide new evidence on the crucial role of L-LecRLKs in later gametophytic pollen development in rice.

The genetic analysis indicated that the male-sterile phenotype of *ap1* appeared to be contributed by the sporophyte (Table S1). It is therefore reasonable to speculate that AP1 may play multiple roles both in sporophytic and gametophytic pollen development. Unexpectedly, we did not find apparently sporophytic defects in the pollen exine and anther wall layers of *ap1* mutant, the classical cell layers for sporophytic abnormalities. It is possible that the sporophytic defects of *ap1* cannot be seen, but are sufficient to alter fertility. Very recently, three other allelic mutants of *AP1* were reported: *s13283* (in the background of the *indica* cultivar Huanghuazhan), *oslecrk5* (in the background of the *japonica* cultivar 02428) and *defective in aperture formation1* (*osdaf1*; in the background of the *japonica* cultivar 9522) (Peng et al., 2019; Wang et al., 2020; Zhang et al., 2020). We carefully compared the cytological characteristics of these allelic mutants and found that they all showed the following identical features: shrinking pollen grains with gametophytic defects (less or no cellular content and absence of pollen intine layer) and sporophytic defects (abnormal aperture morphology). These cytological observations further support the conclusion that AP1 plays a role in pollen starch metabolism during pollen maturation.

However, other sporophytic cellular defects among these allelic mutants were highly variable. For example, the pollen exine was thickened in *s13283* grains (Peng et al., 2019), while the *ap1* (Fig. 6, Fig. S8) and *osdaf1* mutants seemed to display a WT-like pollen exine (Zhang et al., 2020). *oslecrk5* showed impaired formation of the callose layer (Wang et al., 2020), while the *ap1* (Fig. S7) and *osdaf1* mutants displayed no obvious defects in callose deposition during meiosis (Zhang et al., 2020). In *ap1 and oslecrk5* tapetum, the Ubisch bodies appeared denser or smaller than in the WT (Fig. S8D,H) (Wang et al., 2020), while in *s13283* and *osdaf1*, these abnormalities were not obvious (Peng et al., 2019; Zhang et al., 2020). In addition, most of these mutant-specific cellular defects appeared relatively weak. These sporophytically cellular defects might support the hypothesis that the sporophytically male-sterile phenotype of *ap1* is caused by a potentially minor sporophytic defect, such as the denser arrangements of Ubisch bodies. The differently cellular defects of theses mutants can be explained, to some extent, by their different genetic backgrounds. For example, the qRT-PCR analysis revealed that the transcript level of *AP1* reaches two peaks (at stage 8 and stage 11, respectively) during pollen development in *indica* cultivar 9311 (Fig. 4A) and Huanghuazhan (Peng et al., 2019), whereas only one peak (at stage 8) was revealed in *japonica* cultivar 02428 and 9522 (Wang et al., 2020; Zhang et al., 2020). In addition, these diverse expression patterns are generally in accordance with the temporal and spatial occurrence of the cellular defects of the corresponding mutants. Therefore, these data collectively support the multiple roles of *AP1*, both sporophytic and gametophytic, during rice pollen development.

Starch serves as both a sign of pollen maturity and is also a main component of pollen storage materials (Datta et al., 2001). As the source of carbon, sucrose could be metabolized and used for starch synthesis in pollen (Datta et al., 2003). UGP degrades UDP-glucose to produce Glc-1-P, which further serves as the carbon skeleton for starch synthesis (Coleman et al., 2006). Silencing of *OsUPG2*, a member of the rice UGP family, blocked the starch accumulation in pollen, resulting in male sterility (Mu et al., 2009). These findings suggest an essential role for OsUPG2 in pollen starch biosynthesis and pollen maturation. In the present study, the most important finding is that mutation of *AP1* reduced the starch accumulation within pollen (Figs 1, 2, 5, 6 and 7). Two distinctly downregulated phosphorylation sites, located at the UGP domain of OsUPG2, were identified in the *ap1* mutant (Fig. 8D, Fig. S13, Table S3), although the mutation did not cause apparent transcriptional changes of *OsUGP2* (Fig. S14A). Remarkably, both *AP1* and *OsUGP2* are highly co-expressed during late pollen development (Fig. 4, Fig. S14B), which is similar to the phase of pollen starch biosynthesis (Mu et al., 2009). These findings suggest that dysfunction of AP1 might directly lead to the reduced phosphorylation levels of OsUPG2. Consistently, our data indicated that AP1 interacted with and phosphorylated OsUGP2 (Figs 9A-D, 10A), whereas the mutants did not (Figs 9B-D, 10A). Typically, the extracellular domain of RLKs binds the ligands, while the intracellular PK domain regulates the activity of targets through interaction and transphosphorylation (Walker, 1994). Therefore, as an active L-LecRLK, AP1 likely plays a role in pollen starch metabolism through phosphorylation of OsUGP2. Phosphorylated UGPs have been detected during starch accumulation in seeds (Zhang et al., 2014; Pang et al., 2018), suggesting that phosphorylation may be required for maintaining the normal enzymatic activity of OsUGP2 in pollen starch biosynthesis. Consistent with this suggestion, our *in vitro* and *in vivo* assays indicated that the phosphorylation of OsUGP2 by AP1 may enhance OsUGP2 activity (Fig. 10B,C). These findings support the hypothesis that AP1 targets OsUGP2 to exert its role in promoting pollen starch biosynthesis (Fig. S16).

The transcription of many genes associated with sugar and carbohydrate metabolism, as well as sugar signaling, was significantly altered in *ap1*. For example, the expression of a SPS-encoding gene (*LOC_Os01g69030*) was significantly decreased in *ap1* (Fig. 7C,D). SPS proteins play a key role in the complex reaction network of sucrose and starch content. They catalyze a reversible reaction from UDP-Glc and D-fructose-6-phosphate to sucrose-6 phosphate, which is further dephosphorylated to sucrose by sucrose phosphatase (Huber and Israel, 1982; Huber, 1983; Chua et al., 2008). The resultant sucrose can be hydrolyzed to UDP-Glc by SUS for the downstream starch biosynthesis (Karrer and Rodriguez, 1992). As a potent sugar signal in plants, trehalose 6-phosphate (T6P) mediates sucrose use and starch metabolism (Lunn et al., 2006; Martins et al., 2013; Griffiths et al., 2016). T6P is synthesized via T6P synthase (TPS) but dephosphorylated to trehalose and Pi by T6P phosphatase (TPP) (Eastmond and Graham, 2003; Paul, 2007). We observed that the mutation of *AP1* reduced the expression of two TPP genes and two TPS genes, whereas it upregulated the expression of one TPS gene (Fig. 7C,D), indicating an altered T6P homeostasis in *ap1*. HXKs are known sugar sensors that catalyze the conversion of glucose and fructose to hexose 6-phosphates, and play a role in sugar metabolism (Kim et al., 2016). Our data indicated that, in the mutants, *OsHXK7* also showed reduced expression levels (Fig. 7C,D). The control of sucrose cleavage to monomers, sugar signaling and the downstream reactions affect the formation of starch (Kumar et al., 2018), suggesting the perturbed expression levels of these genes may also contribute to the deficient starch accumulation in *ap1* pollen. Considering that AP1 mainly plays a role in post-translational phosphorylation modification, the abnormal expression of *ap1* is likely to be a secondary consequence of its mutation.

Phosphorylation events are involved in the general regulation of starch biosynthesis (Pang et al., 2018). As an active PK, AP1 may modulate the functions of its targets by phosphorylation. The activity of starch synthesis enzymes may be affected by their phosphorylation level (Cohen, 1985). For example, in spinach, the

Development (2021) 148, dev196378. doi:10.1242/dev.196378

change in site-specific phosphorylation of SPS was responsible for the activation state of SPS (Toroser et al., 1999). The enzymatic activity of PGM was enhanced by signaling kinase p21-activated kinase 1 through phosphorylation (Gururaj et al., 2004). Therefore, it is reasonable to propose that the downregulation of phosphorylation may have led to a reduced capacity for metabolic accumulation of sugar and starch, affecting the pollen viability during maturation. Our phosphoproteomic analysis identified downregulated phosphorylation levels of numerous proteins involved in the same pathway (Fig. 8, Table S3). For example, the phosphorylation levels of OspPGM and OsHXK5, which are crucial for pollen sugar metabolism and downstream starch biosynthesis (Lee et al., 2016, 2019), were downregulated in the *ap1* mutant (Table S3). OspPGM and OsHXK5 are located in the plastid (Lee et al., 2016, 2019) (Table S3), suggesting that these two proteins may not directly interact with AP1. Consistently, we did not identify any interactions between AP1 and OspPGM in plant cells (Fig. S17), indicating that AP1 may also indirectly regulate downstream proteins to participate in pollen starch accumulation. In addition, the phosphorylation levels of other proteins that are putatively involved in sugar and starch metabolism, such as disproportionating enzymes (LOC_Os07g46790 and LOC_Os07g43390), SPSs (LOC_Os01g69030 and LOC_Os02g09170) and cytosolic PGM (LOC_Os03g50480), were also downregulated in *ap1* mutant (Table S3). Sugar metabolism and starch biosynthesis require the concerted actions of an extensive range of genes and many sub-functional enzymes (Ball et al., 2011; Hwang et al., 2016), suggesting that, in addition to OsUGP2, AP1 may also affect the phosphorylation levels of other key enzymes, which possibly impact on pollen sugar and starch metabolism. Thus, it will be interesting to reveal how AP1 causes these changes on the expression or phosphorylation of key factors in sugar metabolism and downstream starch biosynthesis.

MATERIALS AND METHODS

Plant materials and growth conditions

The *ap1* plant was isolated from a library of ethyl methyl sulfonate-induced mutants that were generated in a background of the *indica* rice cultivar 9311 (Zou et al., 2017b). For genetic analysis and gene mapping, *ap1* was back-crossed with the WT to produce the F_2 progenies. A *japonica* rice cultivar Nipponbare was used for knocking out *AP1* via the CRISPR/Cas9 system and for the promoter-GUS assay. Rice plants used in this study were grown in the paddy field of Sichuan Agricultural University in Chengdu (Sichuan, China) or in Lingshui (Hainan, China) with routine management.

Morphological and cytological characterization of the mutants

Plants, spikelets and anthers were photographed with a digital camera EOS-1200D (Canon). Pollen viability analysis was performed by staining with FDA and 1% I_2-KI solution, as described previously (Pinillos and Cuevas, 2008; Tao et al., 2019). For anther development analysis, the spikelets with anthers at differently developmental stages were specified according to Tao et al. (2019), and were fixed, dehydrated, embedded, sliced and stained subsequently as described previously (Zou et al., 2017b). The transverse section slides were photographed using an Axio Lab A1 microscope (Zeiss). The detection of chromosome behaviors was carried out according to Yi et al. (2012). For SEM and TEM analysis, anther samples were collected and processed as described by Zou et al. (2018) and then observed with a JSM-7500F SEM (JEOL) or JEM-1400PLUS TEM (JEOL), respectively. Starch measurements were performed as described previously (Zhang et al., 2013).

Molecular cloning of *AP1* and phylogenetic analysis

Leaves of 50 male-sterile mutants in the F_2 progenies were collected for DNA extraction. The extracted DNAs were then pooled and re-sequenced using the Illumina Hiseq platform (Novogene Bioinformatics Technology). Using the MutMap method (Abe et al., 2012), the sequencing results were computationally analyzed. Co-segregation analysis of the candidate mutation in F_2 population was carried out by PCR analysis and sequencing with primer set Seq-AP1. All the primers used in this study are listed in Table S4.

The full-length amino acid sequence of AP1 was used as a query for identifying its plant homologs through the Basic Local Alignment Search Tool in the National Center for Biotechnology Information database (https://blast.ncbi.nlm.nih.gov/Blast.cgi) with default parameters. The proteins with the highest identities to AP1 in each species were considered as the potential AP1 orthologs. Multiple protein alignments and phylogenetic tree constructions were performed using MEGA 5.0 software based on the ClustalW and neighbor-joining method (1000 bootstrap replications), respectively.

CRISPR/Cas9-mediated genomic editing and functional complementation

Specific targets for knocking out of *AP1* by CRISPR/Cas9 system were designed using a CRISPR design tool (http://rice.hzau.edu.cn/cgi-bin/rice2/CRISPR_rice) from Rice Information GateWay. The following CRISPR/Cas9 constructions were performed using the methods described by Miao et al. (2013). A genomic fragment containing 1964 bp promoter region, 2088 bp coding region and 810 bp 3′-untranslated region (UTR) of *AP1* was amplified from Nipponbare, and was thereafter cloned into the binary vector PHB to generate the AP1-com vector. Using the *Agrobacterium*-mediated transformation method with hygromycin B selection (Hiei et al., 1994), the resulting CRISPR/Cas9 constructs were introduced into Nipponbare for knocking out of *AP1*. For functional complementation analysis, the AP1-com vector was introduced into the callus induced by culturing of the young panicles of *ap1* or *cr* homozygous (transgenic-free) plants with Glufosinate selection (Ling et al., 1983; Hiei et al., 1994).

Histochemical GUS assay and RNA *in situ* hybridization

A 1964 bp promoter region of *AP1* was amplified and then cloned into the PHB-GUS vector to generate the $AP1_{pro}$*::GUS* construct, which was further introduced into Nipponbare by *Agrobacterium*-mediated transformation (Hiei et al., 1994). GUS staining was performed as described previously (Zou et al., 2018).

For RNA *in situ* hybridization, templates for the AP1-specific probes were generated using primer set Rish-AP1. The subsequent transcription, labeling and hybridization of probes were performed according to Zou et al. (2017a). Images were obtained using a Zeiss Axio Lab A1 microscope.

RNA-seq and qRT-PCR analysis

Total RNAs were extracted from the specified tissues using an RNeasy Plant Kit (Qiagen). RNA-seq was conducted by Novogene Bioinformatics Technology. More than 6 GB of data were yielded from each sample. Clean data were further analyzed according to Jeong et al. (2016).

The cDNA of extracted RNA was reverse transcribed using NovoScript Reverse Transcriptase (Novoprotein). qRT-PCR was performed on qTOWER3G machine (Analytik-Jena) using AceQ Universal SYBR qPCR Master Mix (Vazyme Biotech) according to the manufacturer's instructions. Relative expression levels were calculated following the $2^{-\Delta\Delta Ct}$ method and using the *Ubiquitin* (*LOC_Os03g13170*, *Ubi*) as the internal reference.

In vitro kinase activity assay

Coding sequences of the intracellular domains of AP1 and *ap1* were amplified with primer set Gex-AP1-C and then cloned into pGEX-4T-1 for fusing in-frame with the GST tag. The point mutation constructs $OsUGP2^{AA}$ and $OsUGP2^{DD}$ were first generated with the Fast Mutagenesis System kit (Transgen) using specific primer pairs. OsUGP2 (including the mutated versions) full-length cDNAs were amplified and then cloned into pET28a for fusing in-frame with the 6×His tag. These constructs were introduced into *Transetta* (DE3) cells (Transgen). Isopropyl-β-D-thiogalactopyranoside (Transgen) was used for induction of protein expression. The recombinant proteins were purified using Mag-Beads GST Fusion Protein Purification kit (Sangon Biotech) or Ni-NTA-Sefinose Colum kit (Sangon Biotech). The *in vitro* phosphorylation assays were

Development (2021) 148, dev196378. doi:10.1242/dev.196378

conducted according to the methods described previously with minor modifications (Zhang et al., 2017). In brief, the recombinant proteins were incubated in the PB [50 mM ATP, 50 mM Tris-HCl (pH 7.5), 10 mM $MgCl_2$, and 1 mM DTT] at 30°C for 2 h. The reaction was stopped by the addition of the 6×Protein Loading Buffer (Transgen). After that, the proteins with or without incubation were separated by SDS-PAGE. The phosphorylation was examined by immunoblotting analysis using anti-phospho (Ser/Thr) Phe antibody (Abcam, ab17464; 1:2000). The input proteins were immunoblotted using anti-GST Tag antibody (Sangon Biotech, D110271; 1:2000) or anti-6×His Tag antibody (Sangon Biotech, D191001; 1:2000).

Phosphoproteomic analysis

Total protein was extracted from the anther samples of the WT and *ap1* following the method described previously (Roy et al., 2007). After trypsin digestion, the resulting peptides were desalted and vacuum dried. The resulting peptides were labeled using the TMT Mass Tagging kit (ThermoFisher Scientific). The TMT-labeled peptides were fractionated into fractions by high pH reverse-phase HPLC. To enrich the phosphopeptides, peptide mixtures were incubated with Ti-IMAC microspheres, and were then collected, washed and eluted according to Tape et al. (2014). The enriched phosphopeptides were further collected and lyophilized, and were then subjected to LC-MS/MS analysis at PTM-BIO Biotechnology to identify the phosphorylation sites and levels.

Y2H assay

Coding sequences of the intracellular domains of AP1 and the full-length OsUGP2 protein were amplified with primer sets AP1-C-BK and OsUGP2-AD, and then cloned into the Y2H bait pGBKT7 and prey pGADT7 vectors, respectively. The prey and bait constructs were co-transformed into *Saccharomyces cerevisiae* strain Y2H gold (Clontech) for performing the Y2H assay according to the manufacturer's instructions.

Subcellular localization and BiFC assay

For subcellular localization, coding sequences (without the stop codon) of the full-length AP1 and OsUGP2 were amplified using the corresponding primer sets. The PCR products of AP1 and OsUGP2 were cloned into the binary vectors PHB-YFP and PHB-CFP for fusing with FP under control of the CaMV35S promoter, respectively. For BiFC assay, the full-length CDS of OsUGP2 was amplified and cloned into a binary vector pXY106 for fusing with N-terminal split nYFP (YN); meanwhile, the CDS encoding full-length AP1 and intracellular domains of AP1 (without the stop codon) was amplified and cloned into a binary vector pXY104 for fusing with C-terminal split-cYFP (YC), respectively. The resultant plasmids were transiently expressed or co-expressed in tobacco leaf epidermis cells or rice protoplasts following the methods described previously (Wang et al., 2013; Lichocka and Schmelzer, 2014). Fluorescent signals were observed using a Nikon A1 fluorescence confocal scanning microscope or Zeiss Axio Imager M2 fluorescence microscope.

LCI assay

The full-length AP1 and the intracellular domains of AP1 or *ap1* were amplified and then cloned into the pCAMBIA1300-nLUC vector for fusing with N-terminal split luciferase (NLuc), respectively, whereas the full-length CDS of OsUGP2 was amplified and cloned into the pCAMBIA1300-nLUC vector for fusing with C-terminal split luciferase (CLuc). OsGIF1 and OsGRF4 proteins (Li et al., 2016) were used as the positive control. LCI assays were performed in tobacco leaves following the protocol described previously (Chen et al., 2008).

In vitro pull-down assay

The recombinant GST-AP1-C or GST-ap1-C fusion proteins were immobilized on Glutathione Magarose Beads (Sangon Biotech) and incubated at room temperature for 30 min. The recombinant His-OsUGP2 protein was then added to the magnetic bead complex and incubated for another 30 min at room temperature. After three times of magnetic bead washing, the magnetic bead complex was subsequently eluted with elution buffer [50 mM Tris-HCl and 10 mM reduced glutathione (pH 8.0)]. The elution components were subjected to immunoblotting analysis using anti-GST tag and anti-His tag antibodies (Sangon Biotech, D110271 and D191001 at 1:2000, respectively).

In vitro UGPase enzyme activity assay

The activity of UGPase was determined according to the protocol described previously (Woo et al., 2008) with slight modifications. Briefly, 0.2 µg of recombinant proteins were added to reaction mixtures (0.2 ml, pH 8) containing 0.2 µmol of UDP-glucose, 0.004 µmol of Glc-1,6-diP, 0.12 µmol of NADP, 1 U of phosphoglucomutase, 1 U of glucose-6-phosphate dehydrogenase, 4 µmol of Cys, 16 µmol of glycylglycine and 1 µmol of $MgCl_2$. Reactions were initiated with the addition of 0.5 µmol inorganic pyrophosphate. In this reaction, the UGPase converts UDP-Glc to Glc-1-P. Then, under the action of the phosphoglucomutase, G-1-P is used to generate glucose-6-phosphate. The resulting glucose-6-phosphate together with NADP are catalyzed by glucose-6-phosphate dehydrogenase to produce gluconolactone-6-phosphate and NADPH. The NADPH formation was monitored continuously at 340 nm and 30°C for 6 h with a molar extinction coefficient of 6.22×10^3 M^{-1} cm^{-1} to reflect the enzyme activity of UGPase.

Determination of starch content in transiently transformed tobacco leaf cells

The full-length CDS sequences of *OsUGP2* (including the mutated versions), *AP1* and *ap1* were amplified and then cloned into a binary vector PHB. The resultant plasmids were transiently expressed or co-expressed in tobacco leaf epidermis cells following the *Agrobacterium* infiltration methods described by Lichocka and Schmelzer (2014). After 48 h of infiltration, the corresponding tobacco leaf area was cut down and ground in liquid nitrogen. The starch content was then examined with the Starch Content Detection Kit (Solarbio).

Acknowledgements

We thank Dr Yangwen Qian (Hangzhou Biogle) for assistance with rice genome editing and transformation.

Competing interests

The authors declare no competing or financial interests.

Author contributions

Conceptualization: S.L.; Methodology: T.Z., L.W.; Software: X.Y., A.W.; Validation: Z.H., Q.X., X.Z.; Formal analysis: Z.H., G.Y., Y.T., H.L.; Investigation: Z.H., Q.X., G.Y., M.L., D.Z., J.Z., Y.L.; Resources: Q.D., A.Z., P.L., S.L.; Data curation: T.Z.; Writing - original draft: T.Z.; Writing - review & editing: S.L.; Visualization: Z.H., Q.X., S.W.; Supervision: P.L., S.L.; Project administration: P.L., S.L.; Funding acquisition: T.Z., Y.L., P.L., S.L.

Funding

This work was supported by the National Natural Science Foundation of China (31971863 to S.L., 31901482 to T.Z., 31700240 to Y.L. and 31971867 to P.L.), by the Open Research Fund of the State Key Laboratory of Hybrid Rice (Hunan Hybrid Rice Research Centre, 2016KF10 to T.Z.), by the Sichuan Science and Technology Support Project (2016NZ0103 and 2017NZDZX0001 to S.L.), and the National Key Research and Development Program of China (2017YFD0100201 to P.L.).

Data availability

The RNA-seq data have been deposited in the NCBI SRA database under accession numbers of SRR11784188 and SRR11784189. The mass spectrometry proteomics data have been deposited with the ProteomeXchange Consortium via the PRIDE partner repository with the dataset identifier of PXD019291.

Supplementary information

Supplementary information available online at
https://dev.biologists.org/lookup/doi/10.1242/dev.196378.supplemental

References

Abe, A., Kosugi, S., Yoshida, K., Natsume, S., Takagi, H., Kanzaki, H., Matsumura, H., Yoshida, K., Mitsuoka, C., Tamiru, M. et al. (2012). Genome sequencing reveals agronomically important loci in rice using MutMap. *Nat. Biotechnol.* **30**, 174-178. doi:10.1038/nbt.2095

Baker, H. G. and Baker, I. (1979). Starch in angiosperm pollen grains and its evolutionary significance. *Am. J. Bot.* **66**, 591-600. doi:10.1002/j.1537-2197.1979.tb06262.x

Ball, S., Colleoni, C., Cenci, U., Raj, J. N. and Tirtiaux, C. (2011). The evolution of glycogen and starch metabolism in eukaryotes gives molecular clues to understand the establishment of plastid endosymbiosis. *J. Exp. Bot.* **62**, 1775-1801. doi:10.1093/jxb/erq411

Barre, A., Hervé, C., Lescure, B. and Rougé, P. (2002). Lectin receptor kinases in plants. *Crit. Rev. Plant Sci.* **21**, 379-399. doi:10.1080/0735-260291044287

Bellande, K., Bono, J.-J., Savelli, B., Jamet, E. and Canut, H. (2017). Plant lectins and lectin receptor-like kinases: how do they sense the outside? *Int. J. Mol. Sci.* **18**, 1164. doi:10.3390/ijms18061164

Borg, M., Brownfield, L. and Twell, D. (2009). Male gametophyte development: a molecular perspective. *J. Exp. Bot.* **60**, 1465-1478. doi:10.1093/jxb/ern355

Börnke, F. and Sonnewald, S. (2011). Biosynthesis and metabolism of starch and sugars. In *Plant Metabolism and Biotechnology* (ed. H. Ashihara, A. Crozier and A. Komamine), pp. 1-25. Wiley. doi:10.1002/9781119991311.ch1

Braun, D. M., Wang, L. and Ruan, Y.-L. (2014). Understanding and manipulating sucrose phloem loading, unloading, metabolism, and signalling to enhance crop yield and food security. *J. Exp. Bot.* **65**, 1713-1735. doi:10.1093/jxb/ert416

Chen, H., Zou, Y., Shang, Y., Lin, H., Wang, Y., Cai, R., Tang, X. and Zhou, J.-M. (2008). Firefly luciferase complementation imaging assay for protein-protein interactions in plants. *Plant Physiol.* **146**, 368-376. doi:10.1104/pp.107.111740

Chourey, P. S., Taliercio, E. W., Carlson, S. J. and Ruan, Y.-L. (1998). Genetic evidence that the two isozymes of sucrose synthase present in developing maize endosperm are critical, one for cell wall integrity and the other for starch biosynthesis. *Mol. Gen. Genet.* **259**, 88-96. doi:10.1007/s004380050792

Chourey, P. S., Jain, M., Li, Q.-B. and Carlson, S. J. (2006). Genetic control of cell wall invertases in developing endosperm of maize. *Planta.* **223**, 159-167. doi:10.1007/s00425-005-0039-5

Chua, T. K., Bujnicki, J. M., Tan, T.-C., Huynh, F., Patel, B. K. and Sivaraman, J. (2008). The structure of sucrose phosphate synthase from Halothermothrix orenii reveals its mechanism of action and binding mode. *Plant Cell.* **20**, 1059-1072. doi:10.1105/tpc.107.051193

Cohen, P. (1985). The role of protein phosphorylation in the hormonal control of enzyme activity. *Eur. J. Biochem.* **151**, 439-448. doi:10.1111/j.1432-1033.1985.tb09121.x

Coleman, H. D., Ellis, D. D., Gilbert, M. and Mansfield, S. D. (2006). Up-regulation of sucrose synthase and UDP-glucose pyrophosphorylase impacts plant growth and metabolism. *Plant Biotechnol. J.* **4**, 87-101. doi:10.1111/j.1467-7652.2005.00160.x

Dangol, S., Singh, R., Chen, Y. and Jwa, N.-S. (2017). Visualization of multicolored in vivo organelle markers for co-localization studies in Oryza sativa. *Mol. cells.* **40**, 828-836.

Datta, R., Chamusco, K. C. and Chourey, P. S. (2003). Starch biosynthesis during pollen maturation is associated with altered patterns of gene expression in maize. *Plant Physiol.* **130**, 1645-1656. doi:10.1104/pp.006908

Datta, R., Chourey, P. S., Pring, D. R. and Tang, H. V. (2001). Gene-expression analysis of sucrose-starch metabolism during pollen maturation in cytoplasmic male-sterile and fertile lines of sorghum. *Sex. Plant Reprod.* **14**, 127-134. doi:10.1007/s00497-001-0105-5

Eastmond, P. J. and Graham, I. A. (2003). Trehalose metabolism: a regulatory role for trehalose-6-phosphate? *Curr. Opin. Plant Biol.* **6**, 231-235. doi:10.1016/S1369-5266(03)00037-2

Eom, J.-S., Chen, L.-Q., Sosso, D., Julius, B. T., Lin, I. W., Qu, X.-Q., Braun, D. M. and Frommer, W. B. (2015). SWEETs, transporters for intracellular and intercellular sugar translocation. *Curr. Opin. Plant Biol.* **25**, 53-62. doi:10.1016/j.pbi.2015.04.005

Esposito, S., Bowsher, C. G., Emes, M. J. and Tetlow, I. J. (1999). Phosphoglucomutase activity during development of wheat grains. *J. Plant Physiol.* **154**, 24-29. doi:10.1016/S0176-1617(99)80313-7

Feng, J., Lu, Y. G., Liu, X.-D. and Xu, X. B. (2001). Pollen development and its stages in rice (Oryza sativa L.). *Chin. J. Rice Sci.* **15**, 21-28.

Griffiths, C. A., Sagar, R., Geng, Y., Primavesi, L. F., Patel, M. K., Passarelli, M. K., Gilmore, I. S., Steven, R. T., Bunch, J., Paul, M. J. et al. (2016). Chemical intervention in plant sugar signalling increases yield and resilience. *Nature.* **540**, 574-578. doi:10.1038/nature20591

Gururaj, A., Barnes, C. J., Vadlamudi, R. K. and Kumar, R. (2004). Regulation of phosphoglucomutase 1 phosphorylation and activity by a signaling kinase. *Oncogene* **23**, 8118-8127. doi:10.1038/sj.onc.1207969

Hiei, Y., Ohta, S., Komari, T. and Kumashiro, T. (1994). Efficient transformation of rice (Oryza sativa L.) mediated by Agrobacterium and sequence analysis of the boundaries of the T-DNA. *Plant J.* **6**, 271-282. doi:10.1046/j.1365-313X.1994.6020271.x

Huber, S. C. (1983). Role of sucrose-phosphate synthase in partitioning of carbon in leaves. *Plant Physiol.* **71**, 818. doi:10.1104/pp.71.4.818

Huber, S. C. and Israel, D. W. (1982). Biochemical basis for partitioning of photosynthetically fixed carbon between starch and sucrose in Soybean (*Glycine max* Merr.) Leaves. *Plant Physiol.* **69**, 691. doi:10.1104/pp.69.3.691

Hwang, S.-K., Koper, K., Satoh, H. and Okita, T. W. (2016). Rice Endosperm Starch Phosphorylase (Pho1) Assembles with Disproportionating Enzyme (Dpe1) to form a protein complex that enhances synthesis of Malto-oligosaccharides. *J. Biol. Chem.* **291**, 19994-20007. doi:10.1074/jbc.M116.735449

Jeong, K., Baten, A., Waters, D. L. E., Pantoja, O., Julia, C. C., Wissuwa, M., Heuer, S., Kretzschmar, T. and Rose, T. J. (2016). Phosphorus remobilization from rice flag leaves during grain filling: An RNA-seq study. *Plant Biotechnol. J.* **15**, 15-26. doi:10.1111/pbi.12586

Karrer, E. E. and Rodriguez, R. L. (1992). Metabolic regulation of rice α-amylase and sucrose synthase genes in planta. *Plant J.* **2**, 517-523. doi:10.1046/j.1365-313X.1992.t01-22-00999.x

Kim, H.-B., Cho, J.-I., Ryoo, N., Shin, D.-H., Park, Y.-I., Hwang, Y.-S., Lee, S.-K., An, G. and Jeon, J.-S. (2016). Role of rice cytosolic hexokinase OsHXK7 in sugar signaling and metabolism. *J. Integr. Plant Biol.* **58**, 127-135. doi:10.1111/jipb.12366

Kumar, R., Mukherjee, S. and Ayele, B. T. (2018). Molecular aspects of sucrose transport and its metabolism to starch during seed development in wheat: A comprehensive review. *Biotechnol. Adv.* **36**, 954-967. doi:10.1016/j.biotechadv.2018.02.015

Lee, S.-K., Hwang, S.-K., Han, M., Eom, J.-S., Kang, H.-G., Han, Y., Choi, S.-B., Cho, M.-H., Bhoo, S. H., An, G. et al. (2007). Identification of the ADP-glucose pyrophosphorylase isoforms essential for starch synthesis in the leaf and seed endosperm of rice (Oryza sativa L.). *Plant. Mol. Biol.* **65**, 531-546. doi:10.1007/s11103-007-9153-z

Lee, S.-K., Eom, J.-S., Hwang, S.-K., Shin, D., An, G., Okita, T. W. and Jeon, J.-S. (2016). Plastidic phosphoglucomutase and ADP-glucose pyrophosphorylase mutants impair starch synthesis in rice pollen grains and cause male sterility. *J. Exp. Bot.* **67**, 5557-5569. doi:10.1093/jxb/erw324

Lee, S.-K., Kim, H., Cho, J.-I., Nguyen, C. D., Moon, S., Park, J. E., Park, H. R., Huh, J. H., Jung, K.-H., Guiderdoni, E. et al. (2019). Deficiency of rice hexokinase HXK5 impairs synthesis and utilization of starch in pollen grains and causes male sterility. *J. Exp. Bot.* **71**, 116-125. doi:10.1093/jxb/erz436

Li, T., Gong, C. and Wang, T. (2010). RA68 is required for postmeiotic pollen development in Oryza sativa. *Plant Mol. Biol.* **72**, 265-277. doi:10.1007/s11103-009-9566-y

Li, S., Gao, F., Xie, K., Zeng, X., Cao, Y., Zeng, J., He, Z., Ren, Y., Li, W., Deng, Q. et al. (2016). The OsmiR396c-OsGRF4-OsGIF1 regulatory module determines grain size and yield in rice. *Plant Biotechnol. J.* **14**, 2134-2146. doi:10.1111/pbi.12569

Lichocka, M. and Schmelzer, E. (2014). Subcellular localization experiments and FRET-FLIM measurements in plants. *Bio-protocol.* **4**, e1018. doi:10.21769/BioProtoc.1018

Ling, D. H., Chen, W. Y., Chen, M. F. and Ma, Z. R. (1983). Direct development of plantlets from immature panicles of rice in vitro. *Plant Cell Rep.* **2**, 172-174. doi:10.1007/BF00270095

Long, W., Dong, B., Wang, Y., Pan, P., Wang, Y., Liu, L., Chen, X., Liu, X., Liu, S., Tian, Y. et al. (2017). FLOURY ENDOSPERM8, encoding the UDP-glucose pyrophosphorylase 1, affects the synthesis and structure of starch in rice endosperm. *J. Plant Biol.* **60**, 513-522. doi:10.1007/s12374-017-0066-3

Lunn, J. E., Feil, R., Hendriks, J. H. M., Gibon, Y., Morcuende, R., Osuna, D., Scheible, W.-R., Carillo, P., Hajirezaei, M.-R. and Stitt, M. (2006). Sugar-induced increases in trehalose 6-phosphate are correlated with redox activation of ADPglucose pyrophosphorylase and higher rates of starch synthesis in Arabidopsis thaliana. *Biochem. J.* **397**, 139-148. doi:10.1042/BJ20060083

Luo, T., Zou, T., Yuan, G., He, Z., Li, W., Tao, Y., Liu, M., Zhou, D., Zhao, H., Zhu, J. et al. (2019). Less and shrunken pollen 1 (LSP1) encodes a member of the ABC transporter family required for pollen wall development in rice (Oryza sativa L.). *Crop J.* **8**, 492-504. doi:10.1016/j.cj.2019.09.001

Ma, H. (2005). Molecular genetic analyses of microsporogenesis and microgametogenesis in flowering plants. *Annu. Rev. Plant Biol.* **56**, 393-434. doi:10.1146/annurev.arplant.55.031903.141717

Mao, G., Meng, X., Liu, Y., Zheng, Z., Chen, Z. and Zhang, S. (2011). Phosphorylation of a WRKY transcription factor by two pathogen-responsive MAPKs drives phytoalexin biosynthesis in *Arabidopsis*. *Plant Cell* **23**, 1639-1653. doi:10.1105/tpc.111.084996

Martins, M. C. M., Hejazi, M., Fettke, J., Steup, M., Feil, R., Krause, U., Arrivault, S., Vosloh, D., Figueroa, C. M., Ivakov, A. et al. (2013). Feedback inhibition of starch degradation in arabidopsis leaves mediated by trehalose 6-phosphate. *Plant Physiol.* **163**, 1142-1163. doi:10.1104/pp.113.226787

McCormick, S. (1991). Molecular analysis of male gametogenesis in plants. *Trends Genet.* **7**, 298-303. doi:10.1016/0168-9525(91)90312-E

McCormick, S. (2004). Control of male gametophyte development. *Plant Cell* **16** Suppl., S142-S153. doi:10.1105/tpc.016659

Miao, J., Guo, D., Zhang, J., Huang, Q., Qin, G., Zhang, X., Wan, J., Gu, H. and Qu, L.-J. (2013). Targeted mutagenesis in rice using CRISPR-Cas system. *Cell Res.* **23**, 1233-1236. doi:10.1038/cr.2013.123

Moon, S., Kim, S.-R., Zhao, G., Yi, J., Yoo, Y., Jin, P., Lee, S.-W., Jung, K.-H., Zhang, D. and An, G. (2013). Rice GLYCOSYLTRANSFERASE1 encodes a glycosyltransferase essential for pollen wall formation. *Plant Physiol.* **161**, 663-675. doi:10.1104/pp.112.210948

Mu, H., Ke, J., Liu, W., Zhuang, C. and Yip, W. (2009). UDP-glucose pyrophosphorylase2 (OsUgp2), a pollen-preferential gene in rice, plays a critical role in starch accumulation during pollen maturation. *Chinese Sci. Bull.* **54**, 234-243. doi:10.1007/s11434-008-0568-y

Okita, T. W. (1992). Is there an alternative pathway for starch synthesis? *Plant Physiol.* **100**, 560-564. doi:10.1104/pp.100.2.560

Oliver, S. N., van Dongen, J. T., Alfred, S. C., Mamun, E. A., Zhao, X., Saini, H. S., Fernandes, S. F., Blanchard, C. L., Sutton, B. G., Geigenberger, P. et al. (2005). Cold-induced repression of the rice anther-specific cell wall invertase gene OSINV4 is correlated with sucrose accumulation and pollen sterility. *Plant Cell Environ.* **28**, 1534-1551. doi:10.1111/j.1365-3040.2005.01390.x

Pang, Y., Zhou, X., Chen, Y. and Bao, J. (2018). Comparative phosphoproteomic analysis of the developing seeds in two Indica rice (Oryza sativa L.) cultivars with different starch quality. *J. Agr. Food Chem.* **66**, 3030-3037. doi:10.1021/acs.jafc.8b00074

Paul, M. (2007). Trehalose 6-phosphate. *Curr. Opin. Plant Biol.* **10**, 303-309. doi:10.1016/j.pbi.2007.04.001

Peng, X., Wang, M., Li, Y., Yan, W., Chang, Z., Chen, Z., Xu, C., Yang, C., Deng, X. W., Wu, J. et al. (2019). Lectin receptor kinase OsLecRK-S.7 is required for pollen development and male fertility. *J. Integr. Plant Biol.* **62**, 1227-1245. doi:10.1111/jipb.12897

Pinillos, V. and Cuevas, J. (2008). Standardization of the fluorochromatic reaction test to assess pollen viability. *Biotech. Histochem.* **83**, 15-21. doi:10.1080/10520290801987204

Riesmeier, J. W., Willmitzer, L. and Frommer, W. B. (1994). Evidence for an essential role of the sucrose transporter in phloem loading and assimilate partitioning. *EMBO J.* **13**, 1-7. doi:10.1002/j.1460-2075.1994.tb06229.x

Roy, S., Sarkar, S. N., Singh, S. K. and Sengupta, D. N. (2007). A dideoxynucleotide-sensitive DNA polymerase activity characterized from endoreduplicating cells of mungbean (Vigna radiata L.) during ontogeny of cotyledons. *FEBS J.* **274**, 2005-2023. doi:10.1111/j.1742-4658.2007.05744.x

Shi, J., Cui, M., Yang, L., Kim, Y.-J. and Zhang, D. (2015). Genetic and biochemical mechanisms of pollen wall development. *Trends Plant Sci.* **20**, 741-753. doi:10.1016/j.tplants.2015.07.010

Tao, Y., Chen, D., Zou, T., Zeng, J., Gao, F., He, Z., Zhou, D., He, Z., Yuan, G., Liu, M. et al. (2019). Defective Leptotene Chromosome 1 (DLC1) encodes a type-B response regulator and is required for rice meiosis. *Plant J.* **99**, 556-570. doi:10.1111/tpj.14344

Tape, C. J., Worboys, J. D., Sinclair, J., Gourlay, R., Vogt, J., McMahon, K. M., Trost, M., Lauffenburger, D. A., Lamont, D. J. and Jørgensen, C. (2014). Reproducible automated phosphopeptide enrichment using magnetic TiO_2 and Ti-IMAC. *Anal. Chem.* **86**, 10296-10302. doi:10.1021/ac5025842

Tetlow, I. J. and Emes, M. J. (2019). Starch biosynthesis in higher plants: the enzymes of starch synthesis. In *Comprehensive Biotechnology* (ed. M. Moo-Young), 3rd edn, pp. 58-76. Elsevier.

Tetlow, I. J., Morell, M. and Emes, M. (2004). Recent developments in understanding the regulation of starch metabolism in higher plants. *J. Exp. Bot.* **55**, 2131-2145. doi:10.1093/jxb/erh248

Tian, X., Li, X., Zhou, W., Ren, Y., Wang, Z., Liu, Z., Tang, J., Tong, H., Fang, J. and Bu, Q. (2017). Transcription factor OsWRKY53 positively regulates brassinosteroid signaling and plant architecture. *Plant Physiol.* **175**, 1337-1349. doi:10.1104/pp.17.00946

Toroser, D., McMichael, R., Krause, K.-P., Kurreck, J., Sonnewald, U., Stitt, M. and Huber, S. C. (1999). Site-directed mutagenesis of serine 158 demonstrates its role in spinach leaf sucrose-phosphate synthase modulation. *Plant J.* **17**, 407-413. doi:10.1046/j.1365-313X.1999.00389.x

Ueda, K., Yoshimura, F., Miyao, A., Hirochika, H., Nonomura, K.-I. and Wabiko, H. (2013). COLLAPSED ABNORMAL POLLEN gene encoding the arabinokinase-like protein is involved in pollen development in rice. *Plant Physiol.* **162**, 858-871. doi:10.1104/pp.113.216523

Vaid, N., Pandey, P. K. and Tuteja, N. (2012). Genome-wide analysis of lectin receptor-like kinase family from Arabidopsis and rice. *Plant Mol. Biol.* **80**, 365-388. doi:10.1007/s11103-012-9952-8

Vaid, N., Macovei, A. and Tuteja, N. (2013). Knights in action: lectin receptor-like kinases in plant development and stress responses. *Mol. Plant.* **6**, 1405-1418. doi:10.1093/mp/sst033

Walker, J. C. (1994). Structure and function of the receptor-like protein kinases of higher plants. *Plant Mol. Biol.* **26**, 1599-1609. doi:10.1007/BF00016492

Wang, K., Liu, Y. and Li, S. (2013). Bimolecular Fluorescence Complementation (BIFC) protocol for rice protoplast transformation. *Bio-protocol.* **3**, e979. doi:10.21769/BioProtoc.979

Wang, B., Fang, R., Zhang, J., Han, J., Chen, F., He, F., Liu, Y.-G. and Chen, L. (2020). Rice OsLecRK5 phosphorylates a UGPase to regulate callose biosynthesis during pollen development. *J. Exp. Bot.* **71**, 4033-4041. doi:10.1093/jxb/eraa180

Wen, L.-Y. and Chase, C. D. (1999). Mitochondrial gene expression in developing male gametophytes of male-fertile and S male-sterile maize. *Sex. Plant Reprod.* **11**, 323-330. doi:10.1007/s004970050159

Woo, M.-O., Ham, T.-H., Ji, H.-S., Choi, M.-S., Jiang, W., Chu, S.-H., Piao, R., Chin, J.-H., Kim, J.-A., Park, B. S. et al. (2008). Inactivation of the UGPase1 gene causes genic male sterility and endosperm chalkiness in rice (Oryza sativa L.). *Plant J.* **54**, 190-204. doi:10.1111/j.1365-313X.2008.03405.x

Yi, J., Kim, S.-R., Lee, D.-Y., Moon, S., Lee, Y.-S., Jung, K.-H., Hwang, I. and An, G. (2012). The rice gene DEFECTIVE TAPETUM AND MEIOCYTES 1 (DTM1) is required for early tapetum development and meiosis. *Plant J.* **70**, 256-270. doi:10.1111/j.1365-313X.2011.04864.x

Zhang, D. B. and Wilson, Z. A. (2009). Stamen specification and anther development in rice. *Chinese Sci. Bull.* **54**, 2342-2353. doi:10.1007/s11434-009-0348-3

Zhang, D. B., Luo, X. and Zhu, L. (2011). Cytological analysis and genetic control of rice anther development. *J. Genet. Genomics.* **38**, 379-390. doi:10.1016/j.jgg.2011.08.001

Zhang, H., Xu, C., He, Y., Zong, J., Yang, X., Si, H., Sun, Z., Hu, J., Liang, W. and Zhang, D. (2013). Mutation in CSA creates a new photoperiod-sensitive genic male sterile line applicable for hybrid rice seed production. *Proc. Natl. Acad. Sci. USA* **110**, 76-81. doi:10.1073/pnas.1213041110

Zhang, Z., Zhao, H., Tang, J., Li, Z., Li, Z., Chen, D. and Lin, W. (2014). A proteomic study on molecular mechanism of poor grain-filling of rice (Oryza sativa L.) Inferior Spikelets. *PLoS ONE* **9**, e89140. doi:10.1371/journal.pone.0089140

Zhang, Z., Li, J., Li, F., Liu, H., Yang, W., Chong, K. and Xu, Y. (2017). OsMAPK3 phosphorylates OsbHLH002/OsICE1 and inhibits its ubiquitination to activate OsTPP1 and enhances rice chilling tolerance. *Dev. Cell* **43**, 731-743.e735. doi:10.1016/j.devcel.2017.11.016

Zhang, X., Zhao, G., Tan, Q., Yuan, H., Betts, N., Zhu, L., Zhang, D. and Liang, W. (2020). Rice pollen aperture formation is regulated by the interplay between OsINP1 and OsDAF1. *Nat. Plants* **6**, 394-403. doi:10.1038/s41477-020-0630-6

Zou, T., He, Z., Qu, L., Liu, M., Zeng, J., Liang, Y., Wang, T., Chen, D., Xiao, Q., Zhu, J. et al. (2017a). Knockout of OsACOS12 caused male sterility in rice. *Mol. Breed.* **37**, 126. doi:10.1007/s11032-017-0722-9

Zou, T., Xiao, Q., Li, W., Luo, T., Yuan, G., He, Z., Liu, M., Li, Q., Xu, P., Zhu, J. et al. (2017b). OsLAP6/OsPKS1, an orthologue of Arabidopsis PKSA/LAP6, is critical for proper pollen exine formation. *Rice*. **10**, 53. doi:10.1186/s12284-017-0191-0

Zou, T., Liu, M., Xiao, Q., Wang, T., Chen, D., Luo, T., Yuan, G., Li, Q., Zhu, J., Liang, Y. et al. (2018). OsPKS2 is required for rice male fertility by participating in pollen wall formation. *Plant Cell Rep.* **37**, 759-773. doi:10.1007/s00299-018-2265-x

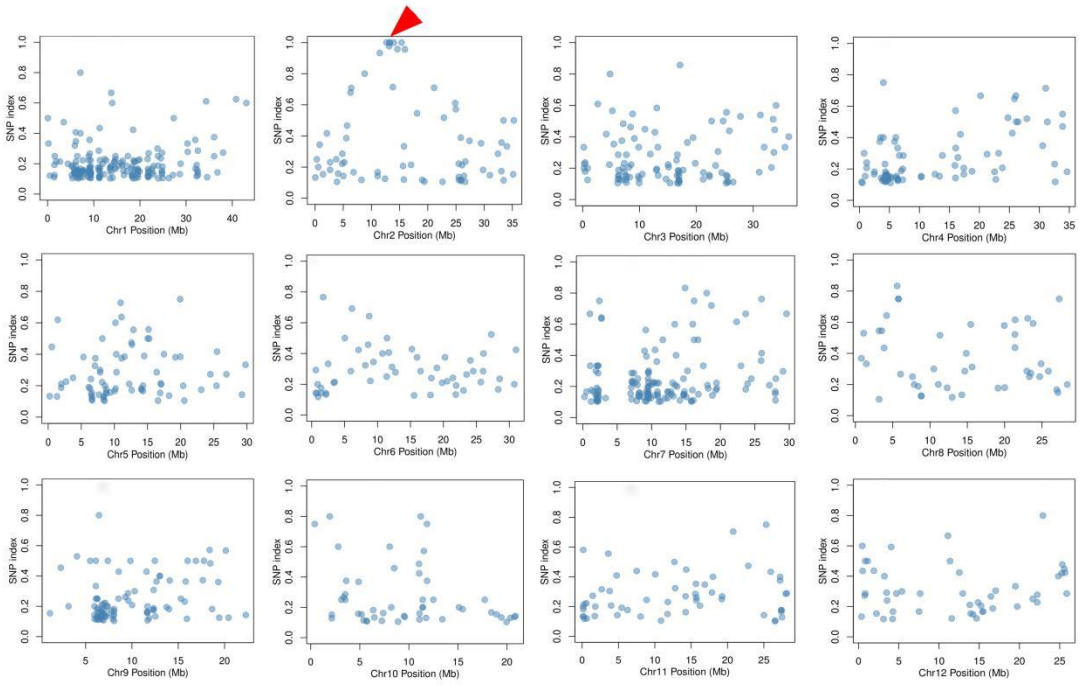

Figure S1. Distributions of SNP index along chromosomes.

The candidate *ap1* mutation on Chromosome 2 is indicated by a red arrow.

Figure S2. Protein sequence alignment of AP1 between the WT and *ap1*.

The sequences were displayed with BOXSHADE.

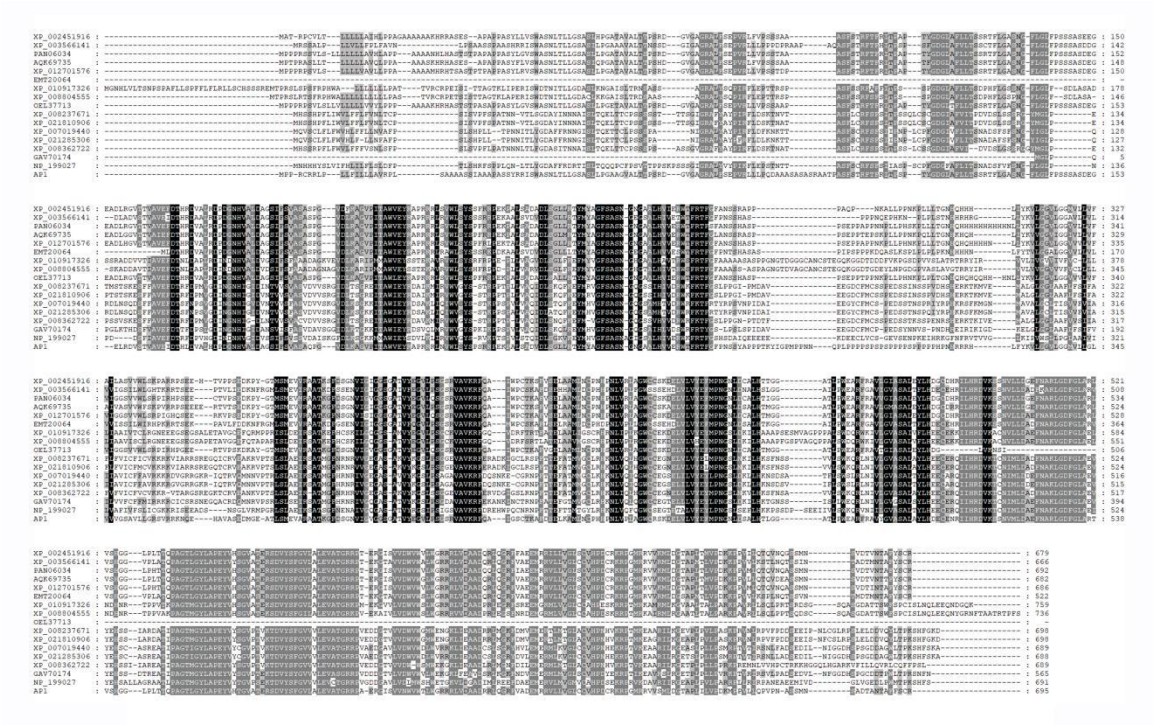

Figure S3. Protein sequences alignment of AP1 and its related homologs in other plant species.

The sequences were displayed with BOXSHADE.

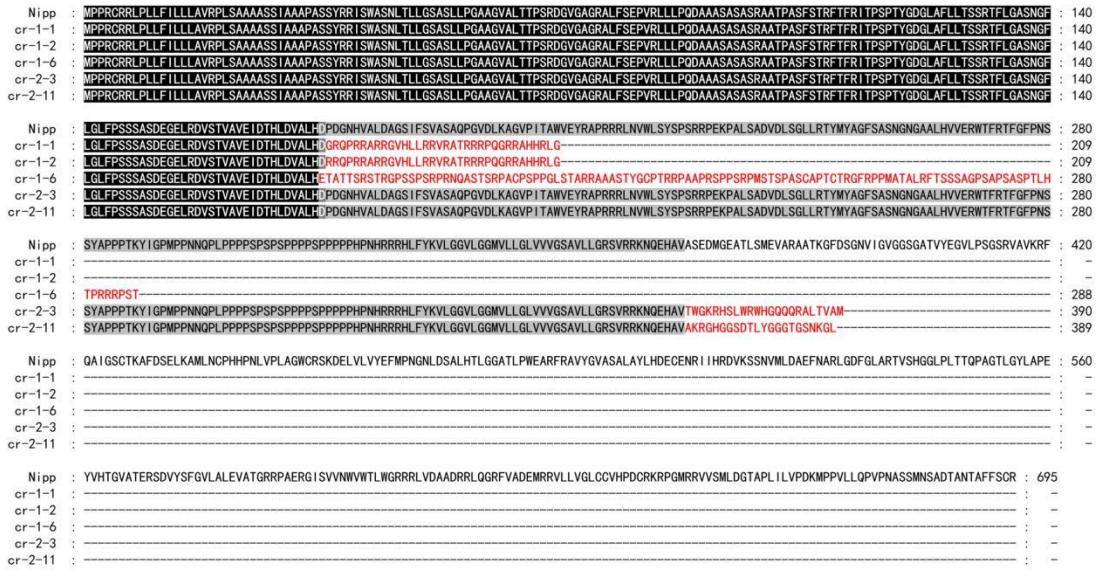

Figure S4. Protein sequences alignment of AP1 between Nipponbare (Nipp) and the CRISPR/Cas9-mediated (*cr*) mutants.

The sequences were displayed with BOXSHADE. The changed amino acids are highlighted by red color.

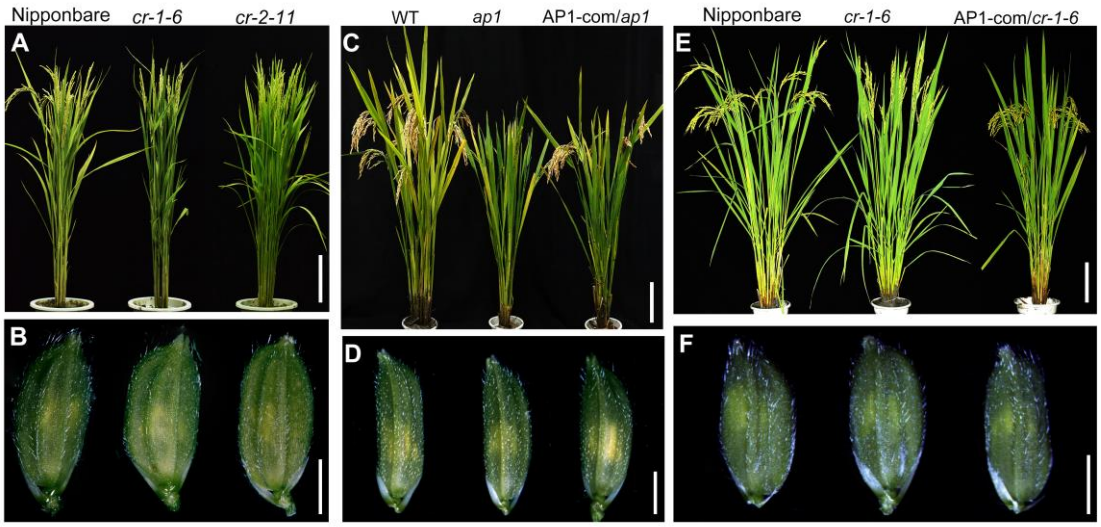

Figure S5. Phenotypic analysis of the CRISPR/Cas9-mediated (*cr*) mutants and the complemented lines.

(A) Mature plants of Nipponbare and the *cr* mutants. (B) Spikelets of Nipponbare and the *cr* mutants at heading stage. (C) Mature plants of the WT, *ap1* mutant and the complemented line (AP1-COM/*ap1*). (D) Spikelets of the WT, *ap1* mutant and the complemented line (AP1-COM/*ap1*) at heading stage. (E) Mature plants of Nipponbare, the *cr* mutant and the complemented line (AP1-COM/*cr-1-6*). (F) Spikelets of Nipponbare, the *cr* mutant and the complemented line (AP1-COM/*cr-1-6*) at heading stage. Scale bars: 15 cm (A, C, E); 2 mm (B, D, F).

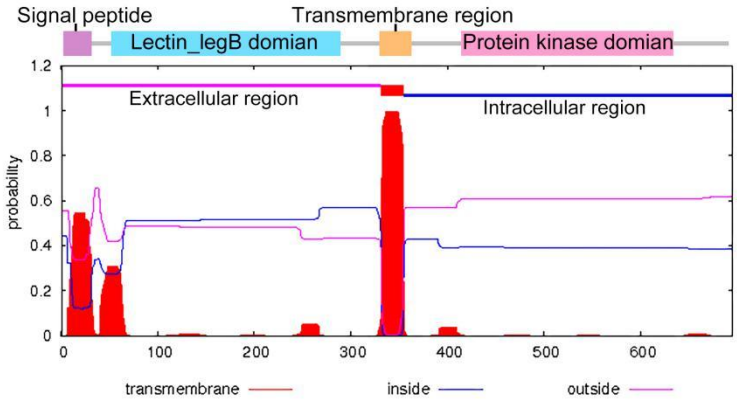

Figure S6. Subcellular localization of AP1 protein domains predicted by TMHMM 2.0.

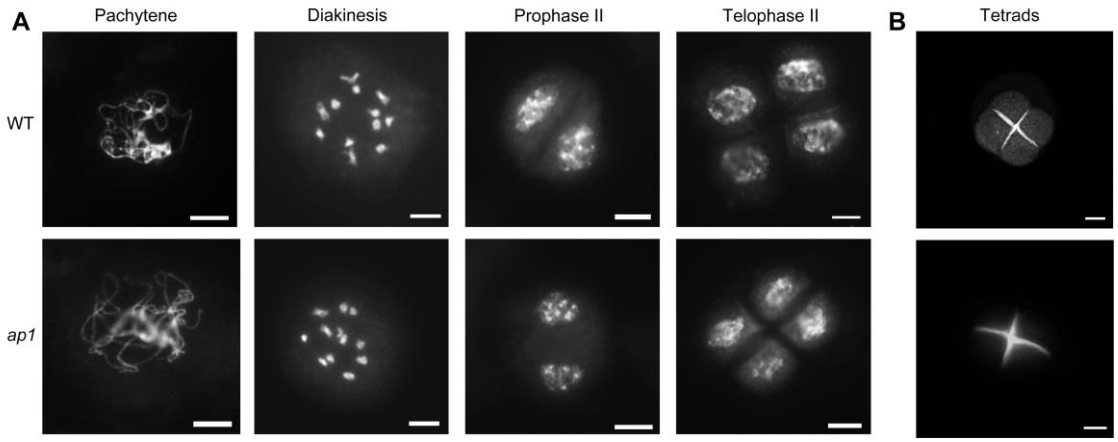

Figure S7. Meiotic processes in the WT and *ap1* anther.

(A) Chromosome behaviors in the WT (upper) and *ap1* (lower) during meiosis. (B) Callose wall of tetrads in the WT (upper) and *ap1* (lower). Scale bars: 10 μm.

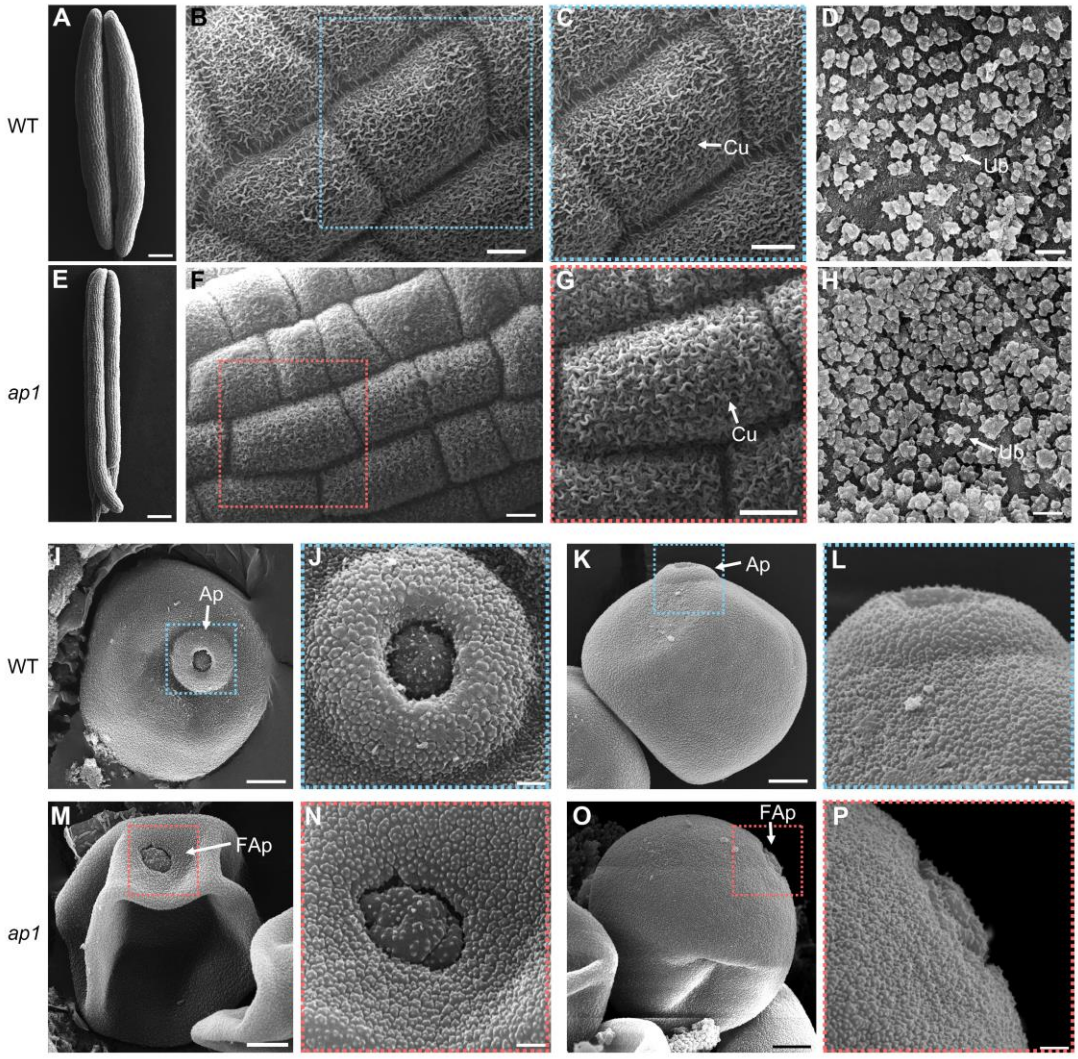

Figure S8. SEM analysis of anther and pollen in the WT and *ap1*.

(A-D, I-L) SEM analysis of the anther and pollen in the WT at stage 12. (E-H, M-P) SEM analysis of the anther and pollen in *ap1* at stage 12. (A, E) Anther. (B, F) Anther outer surface. (C, G) Enlarged images of the anther outer surface in (B) and (F), respectively. (D, H) Anther inner surface. (I, M) Top view of pollen grain. (J, N) Enlarged images of the aperture in (I) and (M), respectively. (K, O) Side view of pollen grain. (L, P) Enlarged images of the aperture in (K) and (O), respectively. Ap, aperture with annulus; Cu, cuticle; FAp, flat aperture lacking annulus. Scale bars: 200 μm (A, E); 10 μm (B, C, F, G); 1 μm (D, H, J, L, N, P); 5 μm (I, L, K, O).

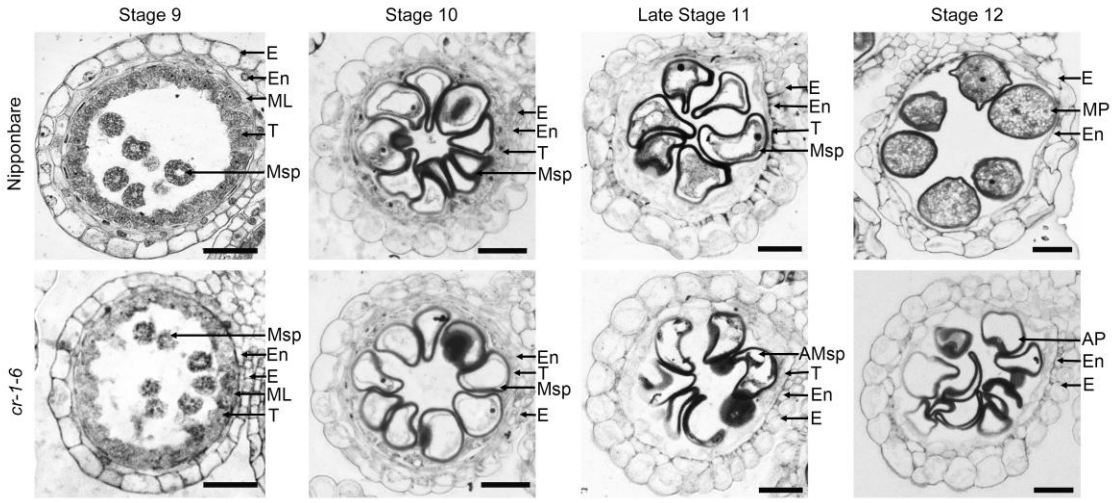

Figure S9. Transverse sections of anthers from Nipponbare (upper) and the CRISPR/Cas9-mediated (*cr*) mutants (lower) at different developmental stages.

AMsp, abnormal microspores; E, epidermis; En, endothecium; AP, abnormal pollen; ML, middle layer; MP, mature pollen; Msp, microspore; T, tapetum. Scale bars: 20 μm.

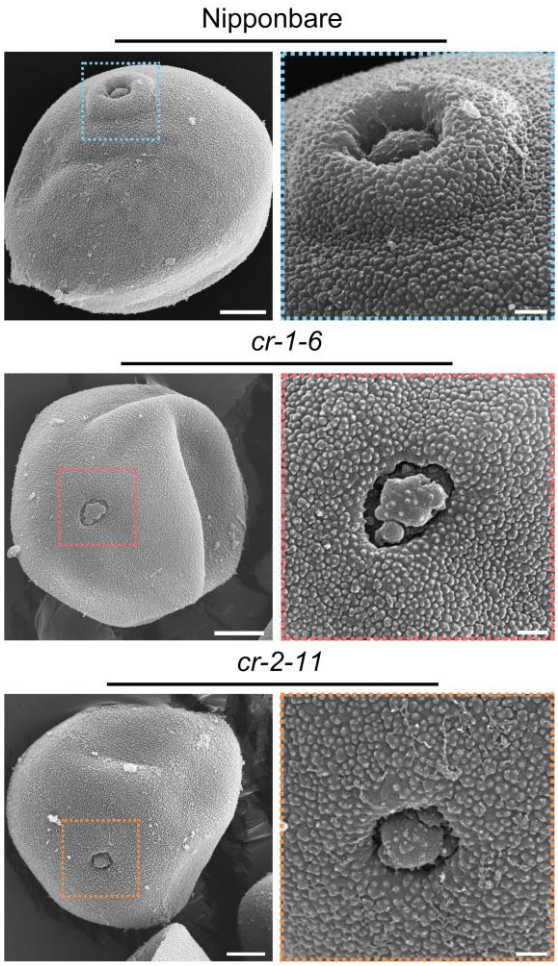

Figure S10. SEM analysis of pollen grains in Nipponbare and the CRISPR/Cas9-mediated (*cr*) mutants.

Enlarged images of the aperture were shown in right panels. Scale bars: 5 μm (the left panels); 1 μm (the right panels).

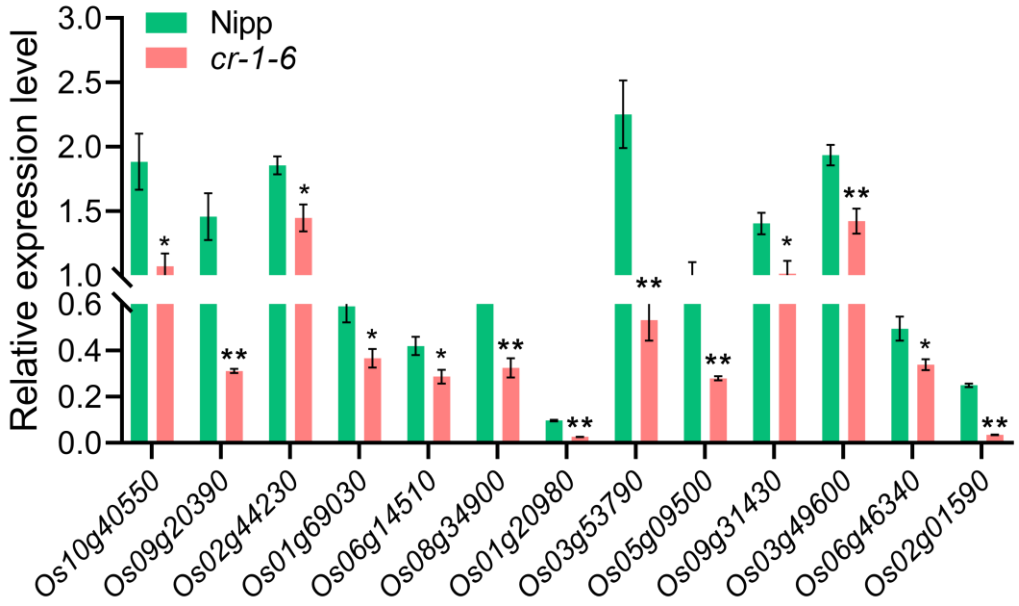

Figure S11. qRT-PCR analysis of several genes related to starch and sucrose metabolism in Fig. 8C

Spikelets of Nipponbare (Nipp) and the CRISPR/Cas9-mediated (*cr*) mutants during the anther stages 11 to 12 were analyzed. Values are means ± SEMof four biological replicates. * and **, statistical significance ($P < 0.05$ and $P < 0.01$) compared with Nipponbare using Student's *t*-test, respectively.

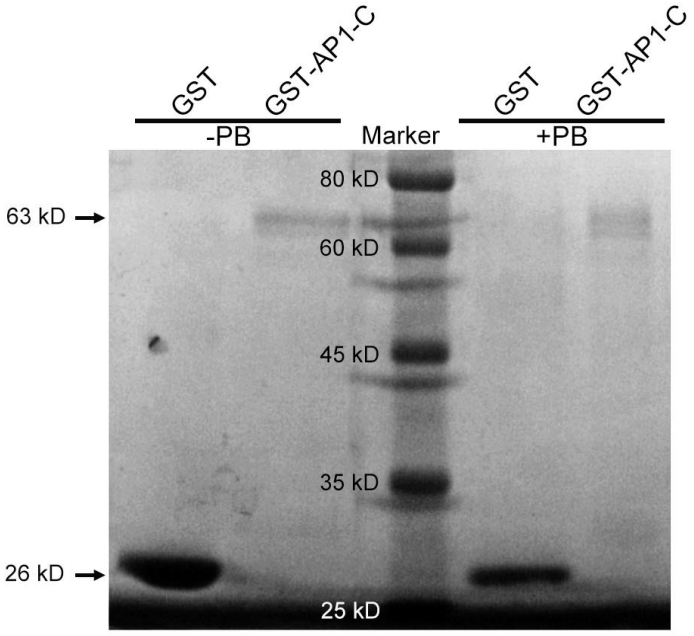

Figure S12. Detection of the recombinant proteins by Coomassie brilliant blue staining.

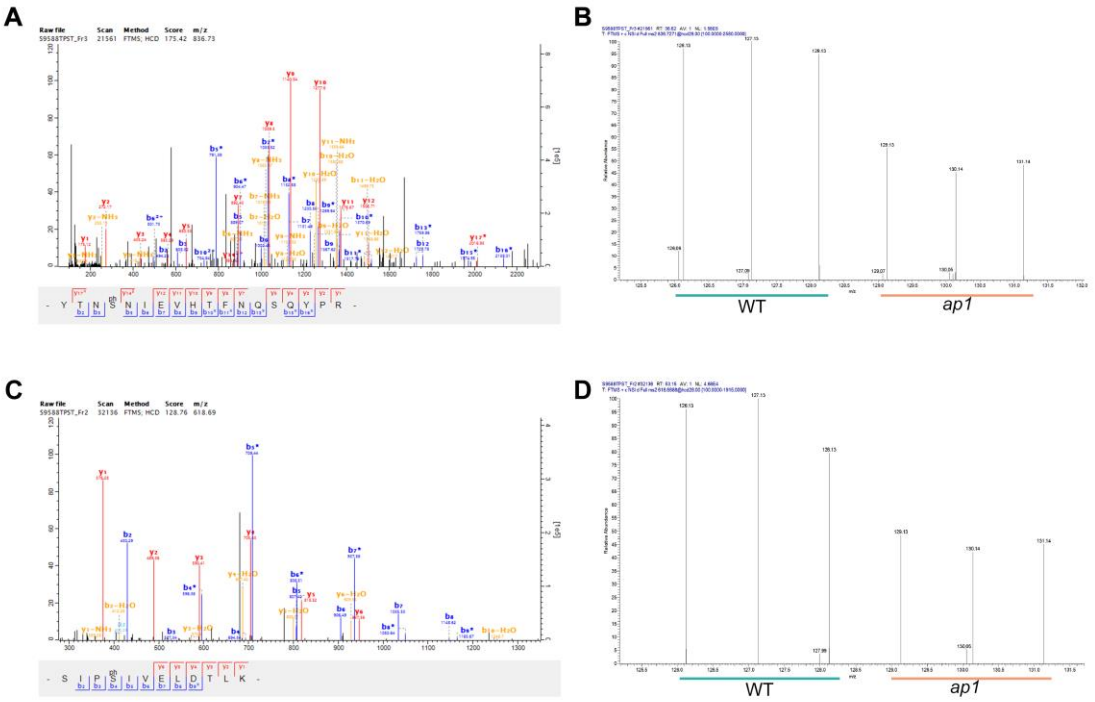

Figure S13. Representative MS/MS spectra for identification of the downregulated phosphorylation sites in OsUGP2.

(A, B) The phosphopeptide YTN**S**NIEVHTFNQSQYPR provides evidence of downregulated phosphorylation of S151. (C, D) The phosphopeptide SIP**S**IVELDTLK provides evidence of downregulated phosphorylation of S413. “b” and “y” denote peptide fragment ions retaining charges at the N-and C- terminus, respectively. The subscript numbers indicate their positions in the identified peptide.

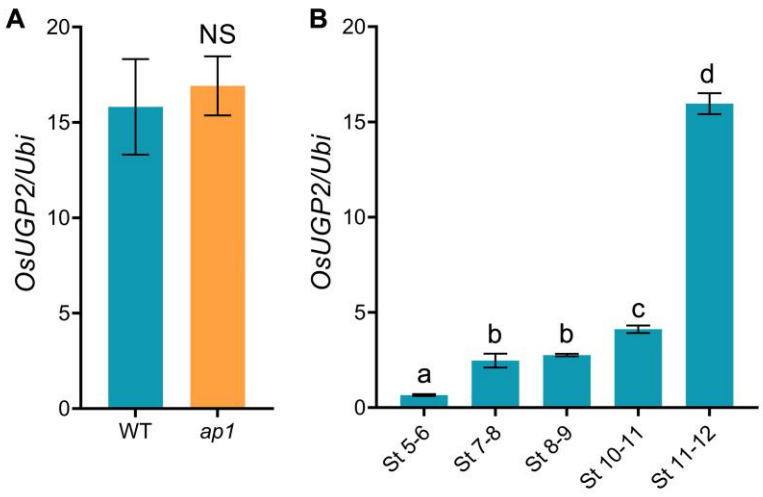

Figure S14. qRT-PCR analysis of *OsUGP2*.

(A) Expression levels of *OsUGP2* in spikelets during the anther stages 11 to 12. Values are means ± SEM of four biological replicates. NS, no significance ($P > 0.05$) compared with the WT using Student's *t*-test. (B) Expression pattern of *OsUGP2* in spikelets. RNAs were extracted from spikelets with anthers at different stages from the WT. Values are means ± SEM of four biological replicates. Statistical significance was determined by Student's *t*-test; significant differences ($P < 0.05$) are indicated by different lowercase letters.

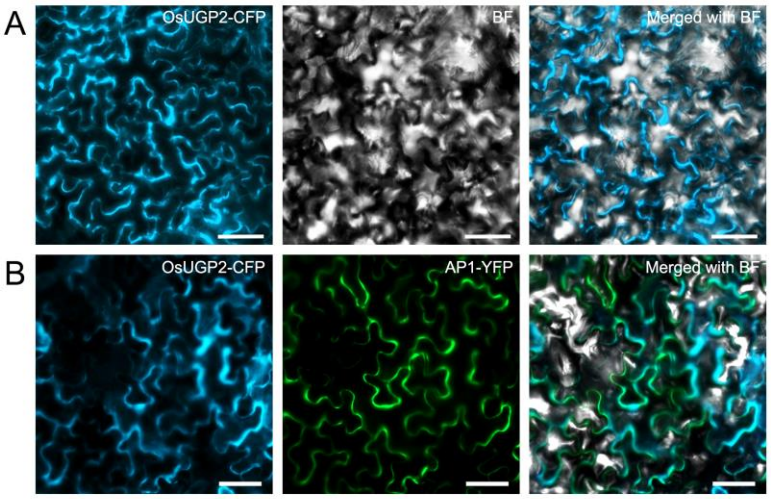

Figure S15. Co-localization of OsUGP2 and AP1 in tobacco leaf epidermis cells.

(A) Subcellular localization of OsUGP2-CFP in tobacco leaf epidermis cells. **(**B) Co-expression of OsUGP2-CFP and AP1-YFP in tobacco leaf epidermis cells. Scale bars: 50 μm.

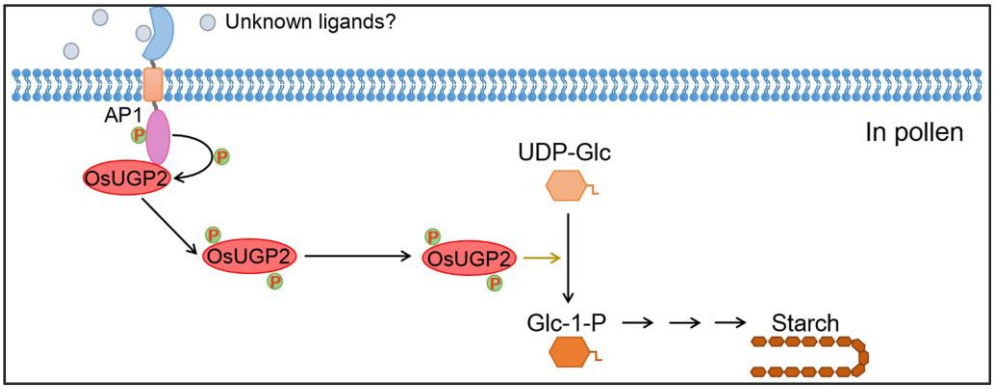

Figure S16. A proposed model for the role of AP1 in pollen starch accumulation.

In pollen, plasma membrane-associated AP1 may receive unknown signals and phosphorylate OsUGP2, which in turn promotes the pollen starch synthesis.

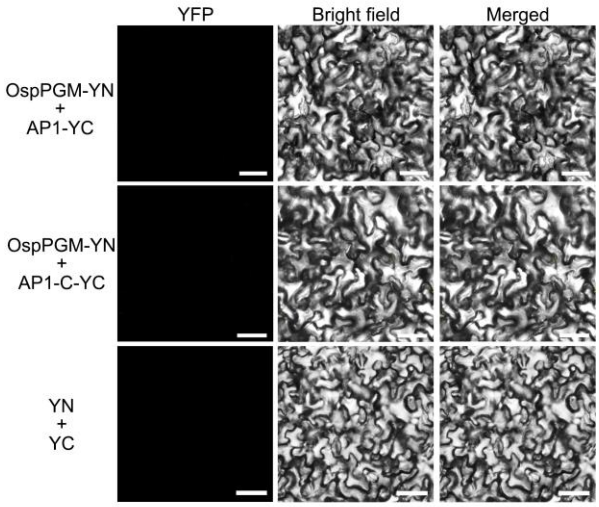

Figure S17. **AP1 could not interact with OspPGM in BiFC assays.**

Scale bars: 50μ m.

Table S1. Segregations of the F_2 population.

Phenotype or genotype	Expected	Observed	c^2	*p* value
Normal-fertility: Male-sterility	3:1	546:154	1.7522	0.1856
AP1/AP1: *AP1/ap1*: *ap1/ap1*	1:2:1	185:361:154	1.7884	0.4089

Table S2. List of SNPs with index of 1 on Chromosome 2.

Position	Base changes	Mutation type	Locus ID	Encoding protein	Effect on amino acids
12668512	A>T	Non-synonymous	*LOC_Os02g21340*	ABC-2 type transporter family protein	F330Y
13175654	G>A	Non-synonymous	*LOC_Os02g22130*	GTPase-activating protein	V113M
13288306	G>A	Intron	*LOC_Os02g22260*	Fruit protein PKIWI502	NA
15365139	C>T	Stop-gained	*LOC_Os02g26160*	Lectin receptor-like kinase	R587*
18116880	C>T	Intergenic	NA	NA	NA

NA, not applicable; *, stop codon.

Table S3. The down-regulated phosphopeptides and corresponding proteins enriched in starch and sucrose metabolism pathway.

Click here to Download Table S3

Table S4. The primers used in this study.

Click here to Download Table S4

Table S5. The unique phosphorylation sites identified from quantitative phosphoproteomic analysis

Click here to Download Table S5